Supporting Online Material

Contents

1 Materials and Methods

1.1 Numerical Methods

1.1.1 Binary Networks

The results in Fig. 2 in the main text were obtained by numerical simulation of binary networks with identical architecture to that studied analytically (see section 2.1), evolving according to the following update rule (see, e.g., (*1*)): on each time step dt, a neuron i out of the $3N$ that compose the network was chosen at random. If this neuron belonged to the external population (X), a random number z was generated and its activity σ_i^X was set to one if $z < \overline{m}_i^X$ and to zero otherwise. In all our simulations, all external neurons had the same mean rate, i.e., $\overline{m}_i^X = m_X$ for all i. If the neuron i to be updated belonged to the recurrent network, its afferent synaptic current was calculated using the instantaneous activity of all other cells in the network which projected to it. If the synaptic current was larger than the firing threshold, its activity σ_i^α was set to one, and otherwise it was set to zero. Using this procedure, each neuron is updated every $3N$ iterations on average, which is defined to be equal to the neuronal time constant τ. Thus, the resolution of the dynamics increases with the network size, i.e., $dt = \tau/3N$. Since neurons from all three populations update their state at this rate, the time constants of the three populations is the same, i.e., $\tau_E = \tau_I = \tau_X = \tau$. The biological interpretation of τ is as the effective time constant with which a neuron changes its firing activity. For concreteness, we assigned it a value of τ = 10 ms throughout this work. In Fig. S4 the time constants of excitatory and inhibitory neurons were different. This was implemented by choosing neurons for update from each population with different probabilities. The firing activity (and synaptic currents) in the network was recorded with a sampling rate SR. The sampling rate was set to $SR = 1/\tau$ when calculating instantaneous correlations and to $SR = 16/\tau$ when calculating lagged correlations. In stationary conditions (Figs. 2 and S4), firing correlations r were calculated as the correlation coefficient of the corresponding strings of 0's and 1's for the given neuronal pair (delayed in the case of lagged correlations). For the case of time-varying external inputs (Fig. S5), the correlation coefficient was calculated between the same strings of 0's and 1's from which the instantaneous time-varying average activity of the cells across trials had been subtracted.

Each dot (curve) in Fig. 2C (2F) is the average over 50 (10) simulations (length 200,000 τ) with different realizations of the connectivity matrix. The parameters we used in all simulations were $p_{\alpha\beta} = p = 0.2$, $m_X = 0.1$, $\theta = 1$, $j_{EE} = 5/\sqrt{N}$, $j_{EI} = -10/\sqrt{N}$, $j_{IE} = 5/\sqrt{N}$, $j_{II} = -9/\sqrt{N}$, $j_{IX} = 4/\sqrt{N}$, $j_{EX} = 5/\sqrt{N}$. The synaptic parameters were chosen so that (apart from the scaling factors) the effective size of a synaptic input $pj_{\alpha\beta}$ would be the same as those used in (*2*). Networks were simulated on two clusters of 28 nodes (http://www.rumba.rutgers.edu/ravana.php) and 19 nodes running Linux, using custom written codes in C, C++.

1.1.2 Integrate-and-fire networks

Figure 1 of main text. We used a simple feed-forward network of current-based leaky integrate-and-fire neurons (*3, 4*) to generate the data in this figure. The subthreshold membrane potential of each post-synaptic neuron evolved according to

$$\tau_m \frac{dV}{dt} \quad = \quad -V + J_E \sum_{i=1}^{N_E} s_i^E(t) - J_I \sum_{i=1}^{N_I} s_i^I(t) \qquad \text{(if } V < \theta\text{)}$$

where $\tau_m = 10$ ms. When $V(t)$ reaches a firing threshold $\theta = 20$ mV the cell fires a spike and it is reset to 10 mV during an absolute refractory period of 2 ms. The synaptic strengths J_α ($\alpha = E, I$) are constants chosen to obtain EPSPs (IPSPs) of peak-amplitude 0.75 (-0.75) mV. PSCs were modeled as a kick followed by an exponential decay,

$$\frac{ds_i^\alpha}{dt} = -s_i^\alpha/\tau_s + \sum_{t_i^\alpha} \delta(t - t_i^\alpha)$$

where the PSC decay time $\tau_s = 5$ ms, $\delta(\ldots)$ is the Dirac delta function and t_i^α are the spike times from pre-synaptic neuron i of population $\alpha = E, I$.

In Fig. 1B we simulated a pair of post-synaptic cells receiving only excitatory spike trains. Each cell received $N_E = 250$ independent Poisson with a constant rate of 5 spikes/s which produced approximatelly the same output rate. A number pN_E of the inputs to each neuron were shared, and p was varied in the range (0, 0.4).

In Fig. 1C, E-F, we fixed the fraction of shared input to $p = 0.2$ and systematically varied the correlation of the input spike trains r_{in}. Besides simulating the case with only excitatory inputs (top trace) we also considered a case with both excitatory ($N_E = 250$) and inhibitory ($N_I = 220$) inputs (bottom curve) with identical spiking statistics. The input firing rate was set to 20 spikes/s to produce an output rate of 5 spikes/s when $r_{in} = 0$. Input spike correlations were generated by the common method of the *mother* train (*5,6*). We first generated a mother Poisson spike train of rate ν/r_{in}. Each pre-synaptic train was a thinned version of the mother train, produced by randomly and independently keeping the spikes of the mother train with probability r_{in}. Finally, each spike in the pre-synaptic trains was jittered by a random interval drawn from a two-tailed exponential distribution of zero mean and a time constant of 5 ms. Thus, all pre-synaptic trains were marginally Poisson, but had (approximately) exponential cross-correlograms of width 10 ms and area r_{in}. Output spike correlations r_{out} were computed numerically as described in section 1.3.4. using a count window $T = 50$ ms and a simulation length L = 10,000 s.

Figure 3 of main text. The results in Fig. 3 were obtained by numerical simulation of spiking conductance-based integrate-and-fire networks (*7–12*) . Except for the sizes of each population, the architecture of the spiking and binary networks was identical. The spiking network was composed of N_E =4000, N_I =1000 and N_X =4000 neurons. The membrane potential V_i^α of the i-th neuron ($i = 1, \ldots, N_\alpha$) from population $\alpha = E, I$ evolves according to

$$C_m \frac{dV_i^\alpha}{dt} = -g_L(V_i^\alpha - V_L) + I_i^{\alpha E}(t) + I_i^{\alpha I}(t) + I_i^{\alpha X}(t) + I_i^{app} \qquad \text{(if } V_i^\alpha < \theta\text{)}$$

where C_m = 0.25 nF is the membrane capacitance, g_L = 16.7 nS is the leak conductance (resting membrane time constant $C_m/g_L = 15$ ms), $V_L = -$ 70 mV is the resting potential and $\theta = -$ 50 mV is

the firing threshold. After a spike, V_i^α was reset to $V_R = -60$ mV during an absolute refractory period of 2 or 1 ms for E and I cells, respectively.

The synaptic currents to this neuron $I_i^{\alpha\beta}$ ($\beta = E, I, X$) are given by

$$I_i^{\alpha\beta}(t) = -\left[\sum_{j=1}^{N_\beta} p_{ij}^{\alpha\beta} g_{ij}^{\alpha\beta} s_{ij}^{\alpha\beta}(t)\right](V_i^\alpha - V_{\rm rev}^\beta)$$

where $V_{\rm rev}^\beta$ is the reversal potential of the corresponding current. We use $V_{\rm rev}^E = V_{\rm rev}^X = 0$ mV and $V_{\rm rev}^I = -80$ mV. The variable $p_{ij}^{\alpha\beta}$ is a binary random variable with probability $p = 0.2$ (except in Fig. S7 D-F) of being equal to one which determines if cell j (in population β) projects to cell i (in population α). The variable $g_{ij}^{\alpha\beta}$ measures the strength of the synaptic conductance between these two cells. All conductance strengths from cells in population β to cells in population α are drawn from Gaussian distributions of mean $g^{\alpha\beta}$ and std. dev. $0.5g^{\alpha\beta}$. We set $g^{EE} = 2.4$ nS, $g^{EI} = 40$ nS, $g^{IE} = 4.8$, nS $g^{II} = 40$ nS, $g^{EX} = g^{IX} = 5.4$ nS. The quantity $s_{ij}^{\alpha\beta}(t)$ represents the instantaneous value of the synaptic gating variable describing the fraction of open channels of the synapse from cell j to cell i. We model unitary conductance changes in response to a pre-synaptic spike as a difference of exponentials:

$$\begin{aligned}
\tau_d \frac{ds_{ij}^{\alpha\beta}}{dt} &= x_{ij}^{\alpha\beta} - s_{ij}^{\alpha\beta} \\
\tau_r \frac{dx_{ij}^{\alpha\beta}}{dt} &= \tilde{\tau} \sum_{t_j^\beta} \delta(t - t_j^\beta - d_{ij}^{\alpha\beta}) - x_{ij}^{\alpha\beta}
\end{aligned}$$

where t_j^β are the spike times of neuron j, $d_{ij}^{\alpha\beta}$ is the conduction delay between the two cells, $\tau_r = 1$ ms and $\tau_d = 5$ ms are the rise and decay times of the unitary conductance change (equal for all synapses in the network, except for Fig. S7 G-I), and the factor $\tilde{\tau} = 1$ ms ensures that the area under the unitary conductance is constant regardless of the rise and decay time-constants. Conduction delays from excitatory (inhibitory) cells were drawn from a uniform distribution $d_{ij}^{\alpha E} = [0.5 : 1.5]$ ms ($d_{ij}^{\alpha I} = [0.1 : 0.9]$ ms) independently for each synapse, sampled at a resolution of 0.05 ms (*13, 14*). Neurons in the external network had Poisson statistics with a constant rate of 2.5 spikes/s (except in Figs. S7 A-C and S8).

In Fig. 3C-D we simulated an intracellular recording where constant currents were injected into cell pairs in which the spiking mechanism had been disabled (*15, 16*). The range of current levels I_{app} was adjusted to isolate EPSPs, IPSPs, or different combinations of EPSPs and IPSPs. The current levels were $I_{app} = -1.3, -0.65, -0.1, 0, 0.2, 0.74, 1.48, 2.22, 2.96, 3.7$ nA. We computed cross-correlograms of the voltages, and obtained for each condition an average over 450 cell pairs from ten different networks (50 s of simulated time) except the EPSP-IPSP condition (Fig. 3C gold curve) were the number of pairs was 1000.

Numerical integration of the differential equations in the simulations was performed using the second-order Runge-Kutta algorithm with an iteration time-step of 0.05 ms, using custom software written in C and C++.

1.2 Experimental Methods

Detailed descriptions of surgery and recording procedures have been published previously (*17–19*). Briefly, nine rats (Sprague-Dawley; 400 - 900 g) were anesthetized with urethane (1.3 - 1.6 g/kg body weight) and ketamine (25-40 mg/kg) plus additional injections of urethane (0.2 g/kg) as needed. In some experiments, cortical inactivation was induced by additional doses of ketamine (10 mg/kg, i.m.). Body temperature was retained with a heating pad. Rats were placed in a stereotaxic frame or naso-orbital restraint, and a window in the scalp was prepared over the somatosensory or auditory cortex. A silicon microelectrode (Neuronexus technologies, Ann Arbor MI) was attached to a micromanipulator and moved gradually to its desired depth position. Probes consisted of eight linearly arranged shanks with 200 μm separation between consecutive shanks (maximal separation was 1.4 mm). Each shank had eight staggered recording sites (20 μm separation). Extracellular signals were high-pass filtered (1 Hz) and amplified (1,000 gain) by using a 64-channel amplifier (Sensorium, Charlotte, VT), and digitized at 25 kHz (DataMax System; RC Electronics, Santa Barbara, CA) or 20 kHz (United Electronic Industries, Inc., Canton, MA). The location of the recording sites was estimated to be layer V by histological reconstruction of the electrode tracks, electrode depth, and firing patterns (*17*). As we observed no significant differences between the auditory and somatosensory data, these were pooled together in the analysis presented in the main text. Data from several of these animals were used in previous studies (*17,18*). All experiments were carried out in accordance with protocols approved by the Rutgers University Animal Care and Use Committee.

1.3 Analysis Methods

1.3.1 Single-Unit Isolation

Units were isolated by a semiautomatic algorithm (http://klustakwik.sourceforge.net) followed by manual clustering (*20*) (http://klusters.sourceforge.net). Single units selected for further analysis had less than 10% contamination in an absolute refractory period of 2 ms and fired more than 75 action potentials in the recording session. Across the 18 recording sessions in 9 rats that we analyzed, an average of 69 (range [16:116], interquartile range [44:93]) simultaneously recorded single units met these conditions.

1.3.2 Classification of cortical state

Under urethane anesthesia, the pattern of cortical background activity spontaneously undergoes transitions (*21–24*) between (i) periods of inactivation (InACT), characterized by global fluctuations in network excitability (Up-states and Down-states) similar to those seen in slow-wave sleep, and (ii) periods of activation (ACT), characterized by tonic activity more similar to REM sleep or attentive wakefulness (*25,26*). Separation into ACT and InACT periods was performed off-line on the basis of the magnitude of the temporal fluctuations in multi-unit activity (MUA, defined as the merged spike trains of all well-isolated units, Fig. S1A). Each recording session was divided into contiguous non-overlapping 10 s intervals and, for each interval, the coefficient of variation (CV) of the spike count of the MUA across 200 windows of $T = 50$ ms was calculated (Fig. S1B). Although cortical activation or inactivation are

associated with lower or higher CV values respectively, the distinction between these two states is not discrete, but rather varies along a continuum (*27*). To highlight the difference in the correlation structure

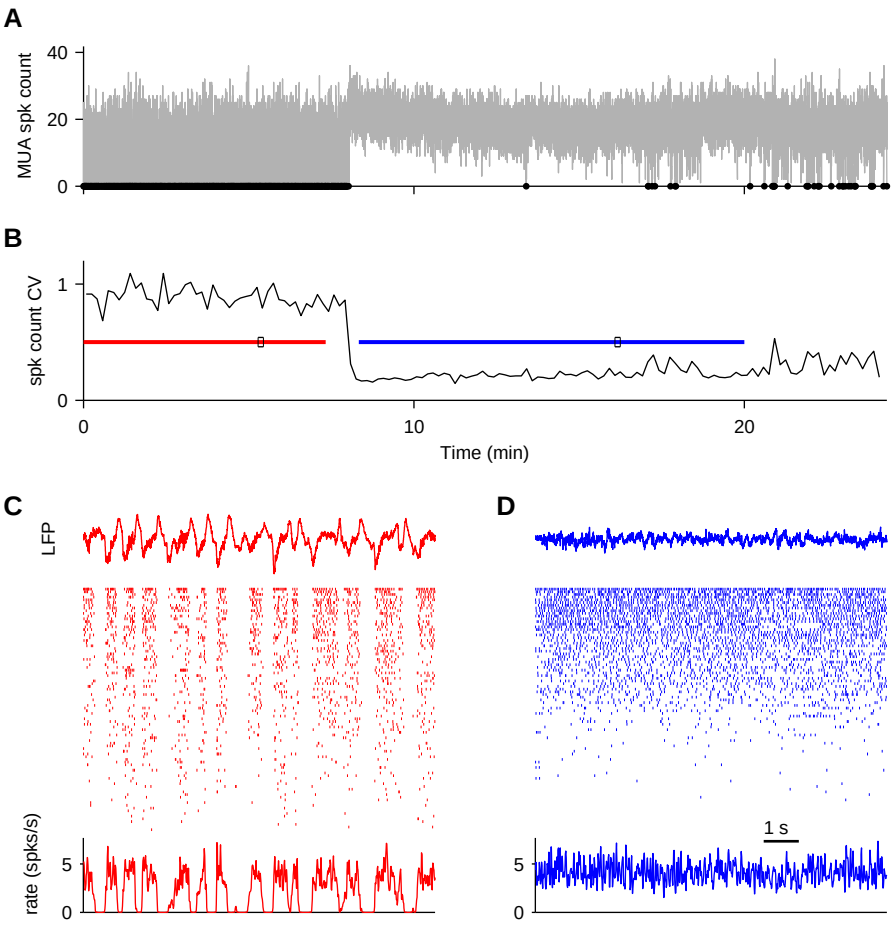

Fig. S1: Classification of cortical state. (A) Evolution of the multi-unit spike count in an example experiment from somatosensory cortex. Gray line is the spike count of the MUA in windows of $T = 50$ ms and black dots indicate the ocurrence of a Down-state (see section 1.3.3). **(B)** Coefficient of variation (CV) of the gray curve in (A) computed in non-overlaping intervals of 10 s. The population recorded makes an abrupt transition from an inactivated state (InACT) to an activated state (ACT) (red and blue bars indicate InACT and ACT periods chosen for further analysis in this particular experiment). **(C-D)** Example local field potential (LFP) traces (top), rasters (middle, cells sorted by rate) and MUA firing rates (bottom, normalized by number of neurons) for 10 s intervals (signaled by the small boxes in (B)) of InACT (C) and ACT (D). During the InACT period, the LFP and MUA rate show large-amplitude, low-frequency fluctuations which are absent during the ACT period.

of neural populations during cortical activation and inactivation, we identified, for each experiment, ACT and InACT periods as those at the extremes of the activation-inactivation continuum, as assessed by the value of the CV of the MUA spike count (Fig. S1B red and blue horizontal bars). Although the

characteristic CV values observed during ACT and InACT periods varied between experiments, all ACT periods had an average CV of less than 0.5, and there was essentially no overlap between the distribution of CVs in the ACT and InACT periods across all experiments. Every period of ACT or InACT had to consist of at least nine consecutive 10 s intervals, and different periods of ACT or InACT in a single experiment were merged. The mean duration of the merged ACT (InACT) period analyzed per recording session was 610s (438s). While sensory stimuli were presented in some experiments, only unstimulated epochs were used for the current analyses.

1.3.3 Detection of Up-states

To isolate intervals of sustained activity (Up-states) during periods of inactivation (InACT), we proceeded by first identifying intervals of silence (Down-states) and then removing them from the spike trains. *Step 1.*- From the MUA spike train, we computed the instantaneous population activity $m(t)$ by convolution with a Gaussian density of width 10 ms. We set a threshold θ at 20% of the maximum of $m(t)$ for the whole recording session, i.e. $\theta = 0.2\, max(m(t))$. *Step 2.*- A Down-state was associated to every inter-spike interval (ISI) in the MUA spike train longer than 50 ms. The Down-state began (ended) at the first point in time left (right) of the center of the ISI where $m(t) = \theta$. *Step 3.*- Every interval in between two Down-states was defined as an Up-state, unless the Up-state was shorter than 50 ms, in which case the two surrounding Down-states were merged together. *Step 4.*- Time-intervals classified as Down-states were removed from all spike spike trains and the correlation coefficient r between the resulting spike trains, composed only of Up-states, were calculated identically as during periods of activation (see next section). Note that, beyond the requirement of a minimum duration of 50 ms, we did not impose any condition of stationarity on Up-states (see, e.g., fluctuations during the third Up-state in Fig. 4C).

1.3.4 Quantifying Spiking Correlations

We quantified spiking correlations using generalized versions of the spike count correlation coefficient, defined as follows. Time was first divided into bins of size $dt = 1$ ms and the spike train from the i-th neuron was represented by a binary sequence $s_i(t)$, equal to 1 if there was a spike in $(t, t + dt)$, and to zero otherwise. The spike count in a window of size T is defined as the number of spikes in $(t, t + T)$, which can be written as a convolution of the spike train with a square kernel of length T. Our measure of the local activity of cell i at time t with resolution T was also a convolution of the spike train with a kernel $K_T(t)$

$$n_i(t;T) \quad = K_T(t) * s_i(t) \quad = \sum_{t'} K_T(t' - t) s_i(t') \tag{1}$$

but we used normalized kernels (area under the kernel equal to one), so the $n_i(t;T)$ have units of firing rate (spks/s). Since the units of $n_i(t;T)$ do not affect any normalized measure of correlation, our results would have been identical had we used spike counts (un-normalized kernels). We used a square kernel (equal to $1/T$ in $(t, t + T)$ and to zero otherwise) when analyzing simulated spiking data (Figs. 1, 3, S6

and S7) and a Gaussian kernel of standard deviation T when analyzing *in vivo* data (Fig. 4, S9 and S11). The results did not qualitatively depend on the choice of kernel.

The statistical properties of spike trains simulated numerically are stationary. Thus, when analyzing simulated data we used the standard expression for the correlation coefficient r_{ij} of the activity of cells i and j

$$r_{ij}(T) = \frac{Cov(n_i, n_j)}{\sqrt{Cov(n_i, n_i)Cov(n_j, n_j)}} \tag{2}$$

where $Cov(n_i, n_j)$ is the covariance between the activity of the two cells

$$Cov(n_i, n_j) = \langle (n_i(t) - \nu_i)(n_j(t) - \nu_j) \rangle = \frac{1}{L} \sum_{t=0}^{L} (n_i(t) - \nu_i)(n_j(t) - \nu_j) \tag{3}$$

and where we have dropped the label T from $n_i(t; T)$ for simplicity. In this case, the mean rate ν_i of the i-th cell is defined as the average of $n_i(t)$ over its whole length L

$$\nu_i = \langle n_i(t) \rangle = \frac{1}{L} \sum_{t=0}^{L} n_i(t) \tag{4}$$

Note that $r_{ij}(T)$ defined in this way, measures the degree to which fluctuations in the activity of the two cells (at temporal resolution T) measured *with respect to* their temporal average across the whole duration of the spike trains (equation (4)) are predictive of each other.

The activity of neurons recorded from a neurophysiological experiment is non-stationary and can, in principle, co-vary on a wide range of time-scales. Changes in the excitability of the local circuit or slow electrode drift can result in coordinated changes in activity over very long time-scales on the order of several minutes. As recognized before (*28*), spiking correlations calculated using the above method in these conditions would likely reflect to a large extent such slow covariations, which we are not the focus of our study. Covariations of a given time-scale (in our case, we are interested in the time-scale of synaptic interactions, i.e., tens of milliseconds) can be isolated by using jitter methods (*29, 30*). The idea is to replace the mean activity of the neuron across the whole recording ν_i in equation (3) by the instantaneous mean $\nu_i(t; J)$ at time t across an ensemble of jittered surrogates of the measured spike trains. In this case, equation (3) reads

$$\begin{aligned} Cov'(n_i, n_j) &= \langle (n_i(t) - \nu_i(t; J))(n_j(t) - \nu_j(t; J)) \rangle \\ &= \frac{1}{L} \sum_{t=0}^{L} (n_i(t) - \nu_i(t; J))(n_j(t) - \nu_j(t; J)) \end{aligned} \tag{5}$$

and

$$\nu_i(t; J) = \frac{1}{N_J} \sum_{k=1}^{N_{jitt}} n_i(t; J_k) \tag{6}$$

where $n_i(t; J_k)$ is the activity at time resolution T (or 'spike count') of the k^{th} jittered version of the recorded spike train $s_i(t)$ at time t and N_{jitt} is the number of jittered surrogates. We jittered spike trains by adding to each spike time an independent Gaussian random variable of zero mean and std. dev. J.

Jittering the spike trains independently by an amount J *only* destroys correlations on time-scales $\ll J$. Thus, since slow covariations (of a time-scale $\gg J$) are present both in the actual data and in the jittered surrogates, non-zero values of equation (5) for a pair of spike trains denote the presence of correlations in their spike trains *only* at time scales $\ll J$. Since we are interested at correlations of time-scale T, in all our analyses we fixed $J = 4T$. In Fig. 4 of the main text, $T = 50$ ms and in Fig. S9, T was varied from 10 to 500 ms. We obtained a normalized correlation (correlation coefficient), by generalizing equation (2)

$$r_{ij}(T) = \frac{Cov'(n_i, n_j)}{\sqrt{Cov'(n_i, n_i)Cov'(n_j, n_j)}} \tag{7}$$

Since we use both a Gaussian kernel $K_T(t)$ and a Gaussian distribution of jitter times, in practice, we calculated $\nu_i(t; J)$ by convolving the measured spike train $s_i(t)$ with a normalized Gaussian kernel of std. dev. $\sqrt{T^2 + J^2}$, which is the asymptotic value of equation (6) as $N_{jitt} \to \infty$. Note that the computation of $Cov'(n_i, n_j)$ simply amounts to the dot product of two time series obtained from the original spike trains by convolution with 'mexican-hat' kernel given by a difference of Gaussians of variances T^2 and $T^2 + J^2$.

The effect of correcting for slow co-modulations of the rates on the computation of $r_{ij}(T)$ can be assessed by examining the cross-correlograms (CCGs) of individual pairs (Fig. S10). Calculating correlations with respect to the mean rate across the recording is equivalent to comparing peaks or troughs in the CCGs with the dashed gray line. Calculating correlations by using the jittered surrogates is equivalent to comparing the CCGs with the red solid line. In most cases the difference between these two ways of estimating correlations is small, but occasionally it is not (some examples are marked by asterisks in Fig. S10).

1.3.5 Assessing significance of correlations

For each population recording, we generated $N_{jitt} = 500$ surrogate data sets. In each surrogate l ($l = 1, \ldots, N_{jitt}$), the spikes times of each of the recorded neurons were jittered by adding a independent Gaussian random variable of zero mean and std. dev. $4T$. In this way, to the measured correlation $r_{ij}(T)$ of each pair ij, we associated N_{jitt} surrogate correlations $r_{\{ij\}_l}(T)$. Note that, by construction, the average of $r_{\{ij\}_l}(T)$ across the distribution of jittered surrogates is zero. We calculated a p-value for the $r_{ij}(T)$ of the original spike trains as

$$\mathrm{p} = (N_{\mathrm{pos}} + N_{\mathrm{neg}})/N_{jitt}$$

where

$$\begin{aligned} N_{\mathrm{pos}} &= \text{number of } r_{\{ij\}_l}(T) > |r_{ij}(T)| \\ N_{\mathrm{neg}} &= \text{number of } r_{\{ij\}_l}(T) < -|r_{ij}(T)| \end{aligned} \tag{8}$$

In Fig. 4 of the main text, the $r_{ij}(T)$ of a pair of spike trains was deemed significant if p < 0.01. We used the same method to assess the significance of the population-averaged correlation $\bar{r}(T)$ (Fig. 4E).

We also calculated the histogram of correlations for each surrogate data set. The white lines in Fig. 4B,D of the main text is the average histogram across the $N_{jitt} = 500$ surrogates. To give an estimate of the variability in the correlation histogram across jittered surrogates, we found, for each value of correlation r, the distribution of values across surrogates of the value of each of the 500 histograms at that value of r. The gray bands in Fig. 4B,D enclose 95% of the mass of the distribution obtained for each value of r.

1.3.6 Cross-correlograms

The value of the raw cross-correlogram (CCG) between a pair spike trains ij was computed following

$$CCG_{ij}(\tau) = \frac{1}{dt^2 L} \sum_{t=0}^{L} \frac{s_i(t) s_j(t+\tau)}{\nu_i \nu_j} \tag{9}$$

where the sum in t runs over time at steps of size dt, L is the number of bins dt in the period (ACT or InACT) and the average rates ν_i are given by equation (4). With this normalization, if the spike trains were independent (on all time-scales) $CCG_{ij}(\tau)$ would be equal to one at all lags τ (except for finite sample fluctuations).

In the insets of Fig. 4B show the average cross-correlograms $CCG_{+}(\tau)$ and $CCG_{-}(\tau)$ over all positively and negatively correlated pairs with p < 0.01, computed as:

$$CCG_{\pm}(\tau) = \frac{1}{N_{\pm}} \sum_{i,j}^{N_{\pm}} CCG_{ij}(\tau), \tag{10}$$

where the sums runs over the N_{+} (N_{-}) positively (negatively) correlated pais with p < 0.01. In this figure we used $dt = 5$ ms.

In Fig. S10 we show individual functions $CCG_{ij}(\tau)$ (white) together with the mean $CCG_{\{ij\}}(\tau)$ (red) obtained for each pair ij by averaging over $N_{jitt} = 1000$ jittered surrogate pairs $\{ij\}_l$ ($l = 1, \ldots, N_{jitt}$) (see above).

1.3.7 Distance-dependence of correlations

We assessed the distance dependence of the mean $\bar{r}$ and standard deviation σ_r of the correlation during periods of activation (Fig. S11). To do this, each pair of spike trains was assigned a distance equal to the distance between the shanks where the two cells were recorded. Pairs recorded in the same shank were assigned a distance equal to zero. We then lumped all pairs with the same distance and recomputed the r histograms for each of the 8 distances in each recording session.

We calculated by a simple linear regression how the particular statistic ($\bar{r}$ or σ_r) depended on the distance between shanks across recording sessions. In order to know whether the slope m_{data} of the

regression was significantly different from zero we used a non-parametric shuffle test. For each statistic, each point was given by a pair (distance-correlation), corresponding, for instance, to the mean correlation of all pairs recorded in the same shank in a given experiment. We created 5000 surrogate data sets by randomly shuffling the distance labels of each point, and calculated the slope of the regression for each surrogate. The p-value reported in the text is the fraction of the surrogates with a slope greater than the absolute value of m_{data} or smaller than minus the absolute value of m_{data}.

2 Analytical description of the recurrent network dynamics

Asynchronous states in recurrent networks have been studied analytically before (*2, 31–38*). However previous treatments lacked at least one of two features which are crucial for an accurate description of how recurrent circuits in the cortex operate: the networks studied so far were either sparsely connected or weakly coupled. In order to make these concepts precise, we adopt the *large* N limit, considering a series of models of increasing size, in which connection probabilities and synaptic strengths scale in a systematic manner with the size N of the network (considering how dynamical properties of the network change with N allows one to make qualitative statements which are robust to changes in the precise values of model parameters). A network is said to have *dense* connectivity if the probability that two cells are connected does not decrease with the network size. In a random densely connected network with connection probability p, pairs of cells will therefore share a fraction p of their inputs on average, even in the limit of very large networks. This should be contrasted to the case of *sparse* connectivity. We say a network is sparsely connected if the average number of pre-synaptic inputs to a neuron is independent of the network size, i.e., if the probability of connection scales as $\sim O(1/N)$. Similarly, a network is said to have *strong* coupling if the number of inputs needed to make the neuron fire is a small fraction of the total number of inputs the cell receives; following (*2*), we assume that this fraction approaches zero as network size increases. Thus, the connection strength has to decrease with the network size at a slower rate than $\sim O(1/N)$. For the current model, we assumed the synaptic couplings scale as $\sim O(1/\sqrt{N})$. With this scaling, the magnitude of temporal fluctuations in the synaptic input currents to the neurons in an asynchronous network saturates to a value of the order of the spiking threshold in the limit of large networks (*2*). Thus, in a densely connected, strongly coupled network, neurons share inputs and synaptic currents display strong temporal fluctuations, even in the limit of very large networks.

Here, we present some aspects of the analysis that we developed to describe asynchronous activity in densely connected, strongly coupled recurrent networks. Our goal is to lay down formally the ingredients necessary to understand the behavior of the population-averaged firing rates and correlations in the stationary self-consistent asynchronous solution. We start in section 2.1 by describing the architecture of the network, and by reviewing the formalism we employed, introduced in (*39*). In section 2.2 we characterize the behavior of firing rates in the asynchronous state. This will later be used to show that the asynchronous state displays tracking of fluctuations. In addition, it generalizes previous work in sparse balanced networks (*2*) to the densely connected case. Our main theoretical result is presented in section 2.3, where we calculate the leading order of the population-averaged pair-wise correlations in the asynchronous state. We show that the leading order is $\sim O(1/N)$, which justifies our claim that the network is asynchronous. In the next sections we illustrate two important properties of the asynchronous solution. First, in section 2.4 we show that the leading-order population averaged correlations just described are equivalent to the tracking of the instantaneous external activity by the excitatory and inhibitory populations, and that tracking becomes more accurate for larger N. The tracking phenomenon is what ensures mechanistically that global fluctuations are not amplified into large network-wide synchrony. We finish this section sketching how to generalize our results (a single network receiving inputs from an external network of independent neurons) to the propagation of activity between several asyn-

chronous networks, thus establishing the full self-consistency of the solution. Second, in section 2.5 we show that the asynchronous solution for the population-averaged correlations is also equivalent to the cancellation of the correlations between the different components of the synaptic currents. This is important because such cancellation can be directly tested experimentally. An illustration of the experiment is performed numerically in Fig. 3C-D of the main text.

2.1 Network Architecture and Dynamics

We consider a recurrent network composed of N excitatory (E) and N inhibitory (I) cells. The probability that a neuron of population $\alpha = E, I$ receives input from a neuron of population $\beta = E, I$ is denoted by $p_{\alpha\beta}$. In addition to the cells in the recurrent network, we also consider input from an external (X) population of neurons, which do not receive inputs from the recurrent network (see Fig. 2A main text). In particular, we assume that there are N excitatory cells in the external network and that the probability of a connection from an external cell to a cell in population α of the recurrent network is $p_{\alpha X}$.

The strength of the synaptic connection from cell j in population β to cell i in population α is denoted as $J_{ij}^{\alpha\beta}$ (Greek letters refer to populations and Latin letters to specific neurons). We consider randomly connected networks in which

$$\begin{aligned} P(J_{ij}^{\alpha\beta} = \frac{j_{\alpha\beta}}{\sqrt{N}}) &= p_{\alpha\beta} \\ P(J_{ij}^{\alpha\beta} = 0) &= 1 - p_{\alpha\beta} \end{aligned} \tag{11}$$

where the quantities $j_{\alpha\beta}$ are order unity (which we write as $\sim O(1)$), meaning that they are independent of the network size. Synaptic connections are thus *strong*. This network architecture is similar to the one analyzed in (*2*), with an important difference. In that network, the average number of pre-synaptic inputs was held fixed independently of the network size, whereas in our network it is a fixed fraction p of the total number of neurons per population N. Thus, in that network the fraction of shared input for any pair of cells vanishes in the limit of large networks, whereas in our network its average is a constant $p_{\alpha\beta}$ independently of the network size.

We use the formalism introduced by Glauber (*39*). This formalism has often been used in neuroscience applications (*1, 40*), including the study of correlations in recurrent networks (*32*) and the analysis of balanced recurrent networks (*2*). In this framework, neurons are modeled as binary elements. We will denote the state at time t of neuron i from population α as $\sigma_i^\alpha(t) = \{0, 1\}$. All neurons update their state independently and stochastically. We will denote as $w(\sigma_i^\alpha)$ the probability per unit time that neuron i from population α changes its state from σ_i^α to $1 - \sigma_i^\alpha$, and by $P(\vec{\sigma}, t)$ the probability that the state of the whole network is $\vec{\sigma} = \{\sigma_i\}$ ($i = 1, \ldots, 3N$) at time t. As described in (*39*), one can write an equation for the rate of change of $P(\vec{\sigma}, t)$ (the master equation) by noting that if neurons update independently, in an infinitesimal interval of length dt, at most one neuron can change its state. If follows that

$$\frac{d}{dt}P(\vec{\sigma}, t) = -P(\vec{\sigma}, t)\sum_i^{N'} w(\sigma_i) + \sum_i^{N'} P(\vec{\sigma}_{(\sigma_i^*)}, t)w(1 - \sigma_i) \tag{12}$$

where $N' \equiv 3N$ and $\vec{\sigma}_{(\sigma_i^*)} = \{\sigma_1, \ldots, 1-\sigma_i, \ldots, \sigma_{N'}\}$. The equation should be solved with the initial condition $\{\vec{\sigma}, 0\}$. Using this equation, one can write up an equation for the temporal evolution of any arbitrary product of neuronal variables. For instance, the temporal evolution of the average activity of neuron i with respect to $P(\vec{\sigma})$ is given by

$$\frac{d}{dt}\langle\sigma_i\rangle(t) \equiv \frac{d}{dt}\left(\sum_{\vec{\sigma}} P(\vec{\sigma},t)\sigma_i\right) = \sum_{\vec{\sigma}}\left(\frac{d}{dt}P(\vec{\sigma},t)\right)\sigma_i$$

Substituting equation (12) into the previous equation, one obtains

$$\frac{d}{dt}\langle\sigma_i\rangle(t) = \sum_{\vec{\sigma}}\left[\sum_{j}^{N'} P(\vec{\sigma}_{(\sigma_j^*)},t)w(1-\sigma_j)\sigma_i - P(\vec{\sigma},t)\sum_{j}^{N'} w(\sigma_j)\sigma_i\right]$$

Since we are summing over all configurations $\vec{\sigma}$, for each term with $\sigma_j = 1$ there is a corresponding term with all other neurons in the same state but $\sigma_j = 0$ and vice-versa. Renaming the dummy indices in the summation over j is therefore equivalent to making the following replacements for the positive terms in the r.h.s of the last equation: when $j \neq i$, $P(\vec{\sigma}_{(\sigma_j^*)},t)w(1-\sigma_j)\sigma_i = P(\vec{\sigma},t)w(\sigma_j)\sigma_i$, and when $j = i$, $P(\vec{\sigma}_{(\sigma_i^*)},t)w(1-\sigma_i)\sigma_i = P(\vec{\sigma},t)w(\sigma_j)(1-\sigma_i)$. The terms with $i \neq j$ cancel with their corresponding negative terms and one is left with

$$\frac{d}{dt}\langle\sigma_i\rangle(t) = \sum_{\vec{\sigma}} P(\vec{\sigma},t)\left[w(\sigma_i)(1-2\sigma_i)\right] \tag{13}$$

Using similar arguments it is straightforward to find the expression for the joint probability that two neurons are active at the same time

$$\frac{d}{dt}\langle\sigma_i\sigma_j\rangle(t) = \sum_{\vec{\sigma}} P(\vec{\sigma},t)\left[w(\sigma_i)(1-2\sigma_i)\sigma_j + w(\sigma_j)(1-2\sigma_j)\sigma_i\right] \tag{14}$$

The dynamics of rates and correlations (of any order) is therefore completely determined by the transition probabilities $w(\ldots)$. In our case they take the form

$$w(\sigma_i^\alpha) = \frac{1}{\tau_\alpha}\left[\sigma_i^\alpha - \Theta(h_i^\alpha)\right]^2 \tag{15}$$

$$w(\sigma_i^X) = \frac{1}{2\tau_X}\left[1 - (2\sigma_i^X - 1)(2\overline{m}_i^X - 1)\right] \tag{16}$$

where $\Theta(\ldots)$ is the Heaviside step function, $\overline{m}_i^X$ is an external parameter specifying the mean activity level of cell i from the external network, and h_i^α is the net afferent current to this cell, given by

$$h_i^\alpha = \sum_{\beta}^{E,I,X}\sum_{j}^{N} J_{ij}^{\alpha\beta}\sigma_j^\beta - \theta_i^\alpha \tag{17}$$

For notational simplicity we have included the threshold θ_i^α of each neuron as a constant negative term in its input current. A neuron's output does not contribute to its input, so the summation in the definition of h_i^α does not include the term proportional to σ_i^α.

According to equation (15), at the time of its update, therefore, a cell from the recurrent network becomes active (inactive) if the afferent input from all other neurons, including the external ones is greater (smaller) than its threshold. According to equation (16), on the other hand, the state to which external cells are updated to does not depend on the state of the rest of the network. Because of this, it will follow that for any given pair of external neurons, $P(\sigma_i^X;\sigma_j^X) = P(\sigma_i^X)P(\sigma_j^X)$. Given the form of the transition probabilities, the symbol $\langle \ldots \rangle$, which stands for an average over the sources of stochasticity in the dynamics, will stand for an average over the distribution of update times of all neurons, and over the probability that an external neuron will become activated when its state is updated.

Let us define the average activity of cell i from population α at time t as $m_i^\alpha(t) = \langle \sigma_i^\alpha \rangle(t)$. Using the transition probabilities (equations (15-16)), equations (13) for the temporal evolution of the average activities become

$$\begin{aligned} \tau_\alpha \frac{d}{dt} m_i^\alpha(t) &= -m_i^\alpha(t) + \langle \Theta(h_i^\alpha(t)) \rangle \\ \tau_X \frac{d}{dt} m_i^X(t) &= -m_i^X(t) + \overline{m}_i^X \end{aligned} \tag{18}$$

Similarly, we define the instantaneous correlation (strictly speaking this is the instantaneous covariance, but we will use the term correlation throughout the description of our analytical results) at time t between units α_i and β_j as

$$r_{ij}^{\alpha\beta}(t) \equiv \langle \delta\sigma_i^\alpha(t) \delta\sigma_j^\beta(t) \rangle \qquad \alpha_i \neq \beta_j$$

where $\delta x \equiv x - \langle x \rangle$ and $\alpha, \beta = E, I, X$. Substituting the transition probabilities in equations (15-16) into equations (13-14) one obtains the following equations for the temporal evolution of the pair-wise correlations

$$\begin{aligned} \tau_{\alpha\beta} \frac{d}{dt} r_{ij}^{\alpha\beta}(t) = -r_{ij}^{\alpha\beta}(t) &+ \frac{\tau_\alpha}{\tau_\alpha + \tau_\beta} \left[\langle \sigma_i^\alpha(t) \Theta(h_j^\beta(t)) \rangle - m_i^\alpha(t) \langle \Theta(h_j^\beta(t)) \rangle \right] \\ &+ \frac{\tau_\beta}{\tau_\alpha + \tau_\beta} \left[\langle \Theta(h_i^\alpha(t)) \sigma_j^\beta(t) \rangle - \langle \Theta(h_i^\alpha(t)) \rangle m_j^\beta(t) \right] \\ \tau_{\alpha X} \frac{d}{dt} r_{ij}^{\alpha X}(t) = -r_{ij}^{\alpha X}(t) &+ \frac{\tau_X}{\tau_\alpha + \tau_X} \left[\langle \Theta(h_i^\alpha(t)) \sigma_j^X(t) \rangle - m_i^\alpha(t) m_j^X(t) \right] \end{aligned}$$

where $\tau_{\alpha\beta} \equiv (\tau_\alpha \tau_\beta)/(\tau_\alpha + \tau_\beta)$. We will be interested in the value of the firing rates and pair-wise correlations in a *stationary* situation (which we will also refer to as equilibrium) where the memory of the initial conditions has been lost and the statistical properties of the network activity are no longer changing. This is equivalent to taking the $t \to \infty$ limit of the previous equations, which results in

$$m_i^\alpha = \langle \Theta(h_i^\alpha) \rangle \tag{19}$$

$$m_i^X = \overline{m}_i^X \tag{20}$$

$$(\tau_\alpha + \tau_\beta) r_{ij}^{\alpha\beta} = \tau_\alpha \langle \delta\sigma_i^\alpha \delta\Theta(h_j^\beta) \rangle + \langle \delta\Theta(h_i^\alpha) \delta\sigma_j^\beta \rangle \tau_\beta \tag{21}$$

$$(\tau_\alpha + \tau_X) r_{ij}^{\alpha X} = \langle \delta\Theta(h_i^\alpha) \delta\sigma_j^X \rangle \tau_X \tag{22}$$

The reason the external-recurrent correlations only contain one term is that neurons from the recurrent network do not project to, and therefore have no influence on, the external neurons.

The difficulty in evaluating this set of coupled non-linear equations lies in the fact that arbitrary dependencies between the activities of different neurons preclude, in principle, a closed form for the probability distribution of the synaptic currents h_i^α. Since the h_i^α are the sum of a large number of stochastic variables, the central limit theorem ensures that, if these variables were independent, the probability distribution of h_i^α would be well approximated by a Gaussian distribution for large networks. However, the existence of shared inputs introduces correlations in the activities of the cells. The central limit theorem can nevertheless still be used if these correlations are sufficiently weak. In fact, if the population-averaged correlations are inversely proportional to the network size N (and higher order cumulants decay fast enough), the distribution of h_i^α can still be well approximated by a Gaussian for large N (*41*). Network states in which the population averaged correlations scale as $\sim O(1/N)$ are called *asynchronous* (*32*). In an asynchronous state, neurons are *effectively* independent (section 3.1), in the sense that the correlations do not significantly impair how well the average firing rate in the network can be estimated (Fig. S2).

Our strategy will therefore be to first *assume* that the network is asynchronous in the steady states. With this assumption, we will develop equations (19-22) to obtain expressions for the population averaged firing rates and pair-wise correlations, in the network. After this, we will show that there are solutions to these equations in which the network is indeed asynchronous.

We will do this in two steps. First, we will develop the set of equations (19-22) without using the fact that the synaptic connections $J_{ij}^{\alpha\beta}$ are stochastic, but using the central limit theorem to invoke a Gaussian distribution for the synaptic currents h_i^α. This leads to a set of coupled equations for the firing rates and pair-wise correlations of each neuron and neuronal pair in the network, which we refer to as the *microscopic* equations. Second, we will average over the distribution of the synaptic connectivity in order to obtain *macroscopic* equations for the *population averaged* firing rates and correlations in the network.

2.2 Firing Rates

We assume that the distribution of the afferent current h_i^α to cell α_i is well approximated by a Gaussian. Let us denote the mean and variance of the the Gaussian distribution of the current to cell α_i at equilibrium by

$$\mu_i^\alpha \equiv \lim_{t\to\infty} \langle h_i^\alpha(t)\rangle \qquad\qquad (s_i^\alpha)^2 \equiv \lim_{t\to\infty} \langle (\delta h_i^\alpha(t))^2\rangle \tag{23}$$

In terms of these quantities, and following the notation in (*42*), equation (19) for the equilibrium firing rate of cell α_i becomes

$$m_i^\alpha = H\left(\psi_i^\alpha\right) \tag{24}$$

where $\psi_i^\alpha \equiv -\mu_i^\alpha/\sqrt{(s_i^\alpha)^2}$ and

$$H(z) \equiv \frac{1}{\sqrt{2\pi}} \int_z^\infty dx \exp(-x^2/2)$$

Equation (24) gives the firing rate of every individual neuron in the network in terms of the activity of all other neurons and the properties of the connectivity. We now would like to obtain a *statistical* descrip-

tion of activity in the network, specifying, for instance, the average firing rate in a given sub-population $m_\alpha \equiv \sum_i m_i^\alpha/N$. In order to do this, one takes advantage of the fact that the network connectivity is stochastic. Because of this, population averages can be thought of as *sample* averages which, if the network is large, will provide accurate estimates of the *distribution* averages induced by the probabilistic connectivity. Let us denote the probability distribution of a given connectivity matrix as $P(J)$. To compute averages over $P(J)$, we note that both the mean μ_i^α and the variance $(s_i^\alpha)^2$ of the current are linear combinations of a large number of uncorrelated random variables (the synaptic variables $J_{ij}^{\alpha\beta}$). Thus, $P(J)$ induces a probability distribution in μ_i^α and $(s_i^\alpha)^2$ which will be well approximated by a Gaussian for large networks. We denote this by

$$\begin{aligned} \mu_i^\alpha &= \mu_\alpha + x_{\mu_\alpha}\Delta\mu_\alpha \\ (s_i^\alpha)^2 &= s_\alpha^2 + x_{s_\alpha^2}\Delta s_\alpha^2 \end{aligned}$$

where the x's are zero-mean, unit-variance Gaussian random variables, and where we have defined $(\Delta a)^2 \equiv [(a-[a])^2]$. We use the notation $[\ldots]$ to denote averages over the distribution of heterogeneity $P(J)$ (*43*). Although the variables x_{μ_α} and $x_{s_\alpha^2}$ are in principle correlated, it can be shown that the cell-to-cell variability in the magnitude of the temporal fluctuations in synaptic current Δs_α^2 decays with the network size, whereas μ_α, $\Delta\mu_\alpha$ and s_α^2 do not. Thus, for large networks, one only needs to consider the following population averages

$$\begin{aligned} \mu_\alpha &= \frac{1}{\epsilon}\sum_\beta J_{\alpha\beta} m_\beta - \theta_\alpha \qquad (25) \\ (\Delta\mu_\alpha)^2 &= \sum_\beta J_{\alpha\beta}^{(2)} q_\beta + \sum_\beta J_{\alpha\beta}^2 (q_\beta - m_\beta^2) \\ s_\alpha^2 &= \sum_\beta J_{\alpha\beta}^{(2)} (m_\beta - q_\beta) + c_{\alpha\alpha} \end{aligned}$$

where we have made the following definitions: $\epsilon \equiv 1/\sqrt{N}$. $J_{\alpha\beta} \equiv [J_{ij}^{\alpha\beta}] = j_{\alpha\beta}p_{\alpha\beta}$ and $J_{\alpha\beta}^{(2)} = [(J_{ij}^{\alpha\beta} - [J_{ij}^{\alpha\beta}])^2] = j_{\alpha\beta}^2 p_{\alpha\beta}(1-p_{\alpha\beta})$. These are, respectively, the average and variance of the distribution of synaptic efficacies between pre-synaptic neurons from population β and post-synaptic neurons from population α. Finally, $q_\alpha \equiv \sum_i (m_i^\alpha)^2/N$ is the second moment of the population distribution of firing rates, and $c_{\alpha\beta} = \sum_{ij}\langle \delta h_i^\alpha \delta h_j^\beta\rangle/N^2$ is the average correlation between the synaptic currents to neurons in populations α and β (*44*). We show below that the population-averaged current correlation decreases with the network size, $c_{\alpha\beta} \sim O(\epsilon)$, so it can also be neglected in the previous equations in the limit of large networks, i.e., as $\epsilon \to 0$. In terms of these quantities, the population-averaged firing rate and the second moment of the rate distribution can therefore be, for large networks, approximated by

$$m_\alpha = \int Dx\, H\left(-\frac{\mu_\alpha + x\Delta\mu_\alpha}{\sqrt{s_\alpha^2}}\right) = H\left(-\frac{\mu_\alpha}{\sqrt{s_\alpha^2 + (\Delta\mu_\alpha)^2}}\right) \qquad (26)$$

$$q_\alpha = \int Dx\, \left[H\left(-\frac{\mu_\alpha + x\Delta\mu_\alpha}{\sqrt{s_\alpha^2}}\right)\right]^2 \qquad (27)$$

where Dx is a Gaussian measure of zero-mean and unit-variance.

As was shown in (*2*), one does not actually have to solve equation (26) in the large N limit in order to obtain the leading order of the firing rates in the network. Because each neuron receives $\sim O(N)$ synaptic inputs, but only $\sim O(\sqrt{N})$ are enough to make it fire, the net magnitude of the total excitation and inhibition felt by the neurons is very large compared to the firing threshold (factor $1/\epsilon$ in the r.h.s. of equation (25)) In order for the firing rates not to be at either zero or at saturation, these large excitatory and inhibitory drives have to cancel, but this cancellation can only happen if the firing rates take on precise values. Thus, for large networks, imposing the cancellation determines the rates. Although this has already been shown in (*2,42*), we briefly now outline the formal derivation of this idea for completeness and because an essentially identical rationale determines the average correlations. In order for the net synaptic input in equation (25) to be of order unity (to avoid complete quiescence or saturation), it has to be true that

$$\sum_{\beta} J_{\alpha\beta} m_\beta = \sum_{\beta=E,I} J_{\alpha\beta} m_\beta + J_{\alpha X} m_X \sim O(\epsilon)$$

Asymptotically, i.e., as $\epsilon \to 0$, this is a linear equation that determines the firing rates at equilibrium

$$\sum_{\beta=E,I} J_{\alpha\beta} m_\beta = -J_{\alpha X} m_X$$

so that

$$m_\alpha = -\sum_{\beta=E,I} J^{-1}_{\alpha\beta} J_{\beta X} m_X \equiv A_\alpha m_X \tag{28}$$

Thus, asymptotically, the population averaged firing rate of each population is proportional to the population averaged rate of the external neurons.

The conditions for this solution to be realized have been described in (*42*). We do not repeat the analysis here, but just mention that the balanced solution is very robust (see also Fig. S4), i.e., it does not require fine-tuned values for any of the network parameters (connection strengths, connection probabilities and neuronal thresholds and time-constants).

2.3 Instantaneous Pair-wise correlations

In order to obtain an expression for the instantaneous pair-wise correlations in equations (21-22) one needs to evaluate terms of the type $\langle \Theta(h_i^\alpha)\sigma_j^\beta \rangle$. Let us first rewrite them in terms of the conditional probability that neuron α_i is active given that neuron β_i is active at the same time. To do this, we note that

$$\begin{aligned}
\langle \Theta(h_i^\alpha)\sigma_j^\beta \rangle &= \sum_{\vec{\sigma}} P(\vec{\sigma})\sigma_j^\beta \Theta(h_i^\alpha) = \sum_{\vec{\sigma}} P(\vec{\sigma}_{(\sigma_j^\beta)}|\sigma_j^\beta) P(\sigma_j^\beta)\sigma_j^\beta \Theta(h_i^\alpha) \\
&= m_j^\beta \sum_{\vec{\sigma}(\sigma_j^\beta)} P(\vec{\sigma}_{(\sigma_j^\beta)}|\sigma_j^\beta = 1)\Theta(h_i^{\alpha}{}_{(\sigma_j^\beta)} + J_{ij}^{\alpha\beta}) = m_j^\beta \langle \Theta(h_i^{\alpha}{}_{(\sigma_j^\beta)} + J_{ij}^{\alpha\beta})|\sigma_j^\beta = 1\rangle
\end{aligned}$$

where $\langle \ldots | \sigma_i = 1 \rangle = \sum_{\vec{\sigma}(\sigma_i)} P(\vec{\sigma}_{(\sigma_i)}|\sigma_i = 1)$ is an average over the conditional distribution of the network activity $\vec{\sigma}$ given that neuron σ_i is active, and $\vec{\sigma}_{(\sigma_i)}$ means that neuron σ_i is excluded from all

those included in $\vec{\sigma}$ (and similarly for $h_i^{\alpha}{}_{(\sigma_j^\beta)}$). The average over the conditional distribution is equivalent to an average over a Gaussian random variable

$$z_i^{\alpha}{}_{(\sigma_j^\beta)} = h_i^{\alpha}{}_{(\sigma_j^\beta)} + J_{ij}^{\alpha\beta}$$

with mean and variance given by

$$\begin{aligned} \overline{\mu}_i^{\alpha} &\equiv \langle z_i^{\alpha}{}_{(\sigma_j^\beta)} | \sigma_j^\beta = 1 \rangle \\ (\overline{s}_i^{\alpha})^2 &\equiv \langle (z_i^{\alpha}{}_{(\sigma_j^\beta)})^2 | \sigma_j^\beta = 1 \rangle - (\overline{\mu}_i^{\alpha})^2 \end{aligned}$$

so that

$$\langle \Theta(h_i^{\alpha}) \sigma_j^\beta \rangle = H(-\overline{\mu}_i^{\alpha} / \sqrt{(\overline{s}_i^{\alpha})^2}) m_j^\beta \tag{29}$$

We develop the previous expression in two steps. First, we relate averages over the conditional distribution to averages over the equilibrium distribution by noting that

$$\begin{aligned} \langle \sigma_i^{\alpha} | \sigma_j^\beta = 1 \rangle &= \langle \sigma_i^{\alpha} (1 + \delta\sigma_j^\beta / m_j^\beta) \rangle \\ \langle \sigma_i^{\alpha} \sigma_k^{\gamma} | \sigma_j^\beta = 1 \rangle &= \langle \sigma_i^{\alpha} \sigma_k^{\gamma} (1 + \delta\sigma_j^\beta / m_j^\beta) \rangle \end{aligned}$$

Second, we relate properties of $h_i^{\alpha}{}_{(\sigma_j^\beta)}$ to properties of h_i^{α} by recalling that

$$\begin{aligned} h_i^{\alpha}{}_{(\sigma_j^\beta)} &= h_i^{\alpha} - J_{ij}^{\alpha\beta} \sigma_j^\beta \\ (h_i^{\alpha}{}_{(\sigma_j^\beta)})^2 &= (h_i^{\alpha})^2 + (J_{ij}^{\alpha\beta} \sigma_j^b)^2 - 2 J_{ij}^{\alpha\beta} h_i^{\alpha} \sigma_j^\beta \end{aligned}$$

which leads to

$$\begin{aligned} \langle z_i^{\alpha}{}_{(\sigma_j^\beta)} | \sigma_j^\beta = 1 \rangle &= \langle h_i^{\alpha} (1 + \delta\sigma_j^\beta / m_j^\beta) \rangle \\ \langle (z_i^{\alpha}{}_{(\sigma_j^\beta)})^2 | \sigma_j^\beta = 1 \rangle &= \langle (h_i^{\alpha})^2 (1 + \delta\sigma_j^\beta / m_j^\beta) \rangle \end{aligned}$$

Using these equations, one can express the conditional rate in terms of the mean μ_i^{α} and variance $(s_i^{\alpha})^2$ of the current over the (unconditional) equilibrium distribution. This is done by noting that

$$\langle (h_i^{\alpha})^2 \delta\sigma_j^\beta \rangle = \langle (\delta h_i^{\alpha})^2 \delta\sigma_j^\beta \rangle + 2 \mu_i^{\alpha} \langle \delta h_i^{\alpha} \delta\sigma_j^\beta \rangle$$

Making the definitions

$$A_{ij}^{\alpha\beta} \equiv \langle \delta h_i^{\alpha} \delta\sigma_j^\beta \rangle \qquad B_{ij}^{\alpha\beta} \equiv \langle (\delta h_i^{\alpha})^2 \delta\sigma_j^\beta \rangle$$

one obtains

$$\begin{aligned} \overline{\mu}_i^{\alpha} &= \mu_i^{\alpha} + (A_{ij}^{\alpha\beta} / m_j^\beta) \\ (\overline{s}_i^{\alpha})^2 &= (s_i^{\alpha})^2 + (B_{ij}^{\alpha\beta} / m_j^\beta) - (A_{ij}^{\alpha\beta} / m_j^\beta)^2 \end{aligned}$$

Equation (29) therefore becomes

$$\langle \Theta(h_i^{\alpha}) \sigma_j^\beta \rangle = H \left(\frac{-\mu_i^{\alpha} - (A_{ij}^{\alpha\beta} / m_j^\beta)}{\sqrt{(s_i^{\alpha})^2 + (B_{ij}^{\alpha\beta} / m_j^\beta) - (A_{ij}^{\alpha\beta} / m_j^\beta)^2}} \right) m_j^\beta \tag{30}$$

If an asynchronous state exists in this network, the population average of the quantities $A_{ij}^{\alpha\beta}/m_j^\beta$ and $(B_{ij}^{\alpha\beta}/m_j^\beta) - (A_{ij}^{\alpha\beta}/m_j^\beta)^2$, which quantify the difference between the conditional and unconditional means and variances to neuron α_i respectively, must be of order $\sim O(1/N)$ at most. Imposing these conditions results in a series of equations that set the value, not only of the population-averaged correlations, but also of a number of other properties of the activity in the network such as the degree to which cells with a higher firing rate tend to have a higher correlation with all other neurons in the network. Here, however, we will only describe how to calculate the population-averaged correlations and firing rates in the network, for which it is sufficient to keep track of terms linear in $A_{ij}^{\alpha\beta}/m_j^\beta$ (*45*). Developing equation (30), thus, up to first order in $A_{ij}^{\alpha\beta}/m_j^\beta$, one obtains

$$\langle \Theta(h_i^\alpha)\sigma_j^\beta \rangle = m_i^\alpha m_j^\beta + \dot{m}_i^\alpha \; A_{ij}^{\alpha\beta} + O((A_{ij}^{\alpha\beta})^2) + O(B_{ij}^{\alpha\beta})$$

where

$$\dot{m}_i^\alpha \equiv \partial m_i^\alpha / \partial \mu_i^\alpha = \partial H(-\mu_i^\alpha / \sqrt{(s_i^\alpha)^2}) / \partial \mu_i^\alpha$$

is the slope of the input-output relationship of the neuron evaluated at the value that the mean current takes in equilibrium. This allows us to write the following expression for the (microscopic) instantaneous correlations at equilibrium

$$(\tau_\alpha + \tau_\beta) r_{ij}^{\alpha\beta} = \dot{m}_i^\alpha A_{ij}^{\alpha\beta} \tau_\beta + \dot{m}_j^\beta A_{ji}^{\beta\alpha} \tau_\alpha \quad (31)$$

$$(\tau_\alpha + \tau_X) r_{ij}^{\alpha X} = \dot{m}_i^\alpha A_{ij}^{\alpha X} \tau_X \quad (32)$$

where

$$A_{ij}^{\alpha\beta} = J_{ij}^{\alpha\beta} m_j^\beta (1 - m_j^\beta) + \sum_{\gamma_k \neq \beta_j} J_{ik}^{\alpha\gamma} r_{kj}^{\gamma\beta} \quad (33)$$

The quantity $A_{ij}^{\alpha\beta}$ measures the influence of pre-synaptic cell β_j on the firing of post-synaptic cell α_i. The first term in $A_{ij}^{\alpha\beta}$ contains the contribution of a direct connection from cell β_j to cell α_i to their pair-wise correlation. This effect is also proportional to the temporal variance of the pre-synaptic cell $m_j^\beta(1-m_j^\beta)$. The second term contains the contributions of all those cells which project to the post-synaptic cell α_i and with which the pre-synaptic cell β_j is correlated.

We would now like to obtain expressions for the population-averaged correlations $r_{\alpha\beta} \equiv \sum_{ij} r_{ij}^{\alpha\beta}/N^2$ (if $\alpha = \beta$ in the previous expression, the pre-factor should be $[N(N-1)]^{-1}$). As described above, we will do this by averaging over the distribution of randomly connected networks $P(J)$, again assuming that dynamical properties and functions of $J_{ij}^{\alpha\beta}$ factorize under $P(J)$. Let us start with the external-recurrent correlations in equation (32). Averaging over $P(J)$ one gets

$$(\tau_\alpha + \tau_X) r_{\alpha X} = \left[\epsilon \, \tilde{J}_{\alpha X} a_X + \frac{1}{\epsilon} \sum_{\gamma = E,I} \tilde{J}_{\alpha\gamma} r_{\gamma X} \right] \tau_X \quad (34)$$

where $a_X \equiv m_X - q_X$ and $\tilde{J}_{\alpha\beta} \equiv \dot{m}_\alpha J_{\alpha\beta}$, with $\dot{m}_\alpha \equiv [\dot{m}_i^\alpha] = \partial m_\alpha / \partial \mu_\alpha$. In the last section, we saw that due to the strong connectivity, there was a mismatch between the magnitude of the net input to

the neurons and their activity unless there was a precise cancellation of net excitation and inhibition. A similar situation takes place here. Even if we assume that the network is indeed asynchronous, so that all population averaged correlations scale as $r_{\alpha\beta} \sim O(\epsilon^2)$, the l.h.s. of the previous equation is $\sim O(\epsilon^2)$ and the r.h.s is $\sim O(\epsilon)$. Thus, the equation has no solution unless there is a precise cancellation between the different terms in the r.h.s. To reveal this explicitly, we express $r_{\gamma X}$ as a Taylor series in ϵ

$$r_{\gamma X} = \sum_{n=0} r_{\gamma X}^{(n)} \epsilon^n$$

substitute this expression in equation (34) and evaluate the equation at each order in ϵ separately. Doing this shows that the first non-zero term in the series is $r_{\gamma X}^{(2)}$, whose value is given by the solution of

$$\sum_{\gamma=E,I} \tilde{J}_{\alpha\gamma} r_{\gamma X}^{(2)} + \tilde{J}_{\alpha X} a_X = 0 \quad \longrightarrow \quad r_{\gamma X}^{(2)} = -\sum_{\alpha=E,I} \tilde{J}_{\gamma\alpha}^{-1} \tilde{J}_{\alpha X} a_X = A_\gamma a_X \tag{35}$$

The last equality follows from the fact that

$$\sum_{\alpha=E,I} \tilde{J}_{\gamma\alpha}^{-1} \tilde{J}_{\alpha X} = \sum_{\alpha=E,I} J_{\gamma\alpha}^{-1} J_{\alpha X} \equiv -A_\gamma$$

Thus, we have shown that

$$r_{\alpha X} = \epsilon^2 A_\alpha a_X + O(\epsilon^3)$$

Using similar arguments, equation (31) can be written as

$$\begin{aligned}(\tau_\alpha + \tau_\beta) r_{\alpha\beta} = \epsilon\, \tilde{J}_{\alpha\beta} a_\beta \tau_\beta \quad &+ \quad \frac{1}{\epsilon}\left[\sum_{\gamma=E,I} \tilde{J}_{\alpha\gamma} r_{\gamma\beta} + \tilde{J}_{\alpha X} r_{X\beta}\right]\tau_\beta + \\ \epsilon\, \tilde{J}_{\beta\alpha} a_\alpha \tau_\alpha \quad &+ \quad \frac{1}{\epsilon}\left[\sum_{\gamma=E,I} \tilde{J}_{\beta\gamma} r_{\gamma\alpha} + \tilde{J}_{\beta X} r_{X\alpha}\right]\tau_\alpha\end{aligned} \tag{36}$$

Again, expanding the $r_{\alpha\beta}$ and a_α in powers of ϵ and evaluating the previous equation at each order, the term $\sim O(\epsilon)$ results in the following equation

$$\tilde{J}_{\alpha\beta} a_\beta^{(0)} \tau_\beta + \left[\sum_{\gamma=E,I} \tilde{J}_{\alpha\gamma} r_{\gamma\beta}^{(2)} + \tilde{J}_{\alpha X} r_{X\beta}^{(2)}\right]\tau_\beta + \tilde{J}_{\beta\alpha} a_\alpha^{(0)} \tau_\alpha + \left[\sum_{\gamma=E,I} \tilde{J}_{\beta\gamma} r_{\gamma\alpha}^{(2)} + \tilde{J}_{\beta X} r_{X\alpha}^{(2)}\right]\tau_\alpha = 0$$

where $a_\alpha^{(0)} = m_\alpha^{(0)} - q_\alpha^{(0)}$ is the leading-order population-averaged temporal variance of the activity of cells in population α. In the general case, the solution to the previous equation is that the first three and last three terms in the last equation (which are identical if we exchange the values of α and β) are both equal to zero, i.e., $r_{\alpha\beta}^{(2)}$ is the solution of

$$\sum_{\gamma=E,I} \tilde{J}_{\beta\gamma} r_{\gamma\alpha}^{(2)} + \tilde{J}_{\beta X} r_{X\alpha}^{(2)} + \tilde{J}_{\beta\alpha} a_\alpha^{(0)} = 0$$

It is useful to define the correlation $v_{\alpha\beta}$ between the instantaneous activity of populations α and β at equilibrium. Using the notation $\delta_{\alpha\beta}$ for the Kronecker delta, $v_{\alpha\beta}$ is given by

$$v_{\alpha\beta} = \lim_{t\to\infty} \langle \sum_i (\delta\sigma_i^\alpha(t)/N) \sum_j (\delta\sigma_j^\beta(t)/N) \rangle = r_{\alpha\beta} + \epsilon^2 \delta_{\alpha\beta} a_\alpha \tag{37}$$

in terms of which the previous equation can be written as

$$\sum_{\gamma=E,I} \tilde{J}_{\beta\gamma} v_{\gamma\alpha}^{(2)} + \tilde{J}_{\beta X} r_{X\alpha}^{(2)} = 0 \quad \longrightarrow \quad v_{\gamma\alpha}^{(2)} = -\sum_{\beta=E,I} \tilde{J}_{\gamma\beta}^{-1} \tilde{J}_{\beta X} r_{X\alpha}^{(2)} = A_\gamma A_\alpha a_X$$

The solution for the population-averaged instantaneous pair-wise correlations in the steady states in our network is therefore

$$\begin{aligned}
r_{EX} &= \epsilon^2 A_E a_X + O(\epsilon^3) \\
r_{IX} &= \epsilon^2 A_I a_X + O(\epsilon^3) \qquad (38) \\
r_{EE} &= \epsilon^2 (A_E^2 a_X - a_E^{(0)}) + O(\epsilon^3) \\
r_{II} &= \epsilon^2 (A_I^2 a_X - a_I^{(0)}) + O(\epsilon^3) \\
r_{EI} &= \epsilon^2 A_E A_I a_X + O(\epsilon^3) \qquad (39)
\end{aligned}$$

2.4 Tracking of fluctuations in the asynchronous state

There is a simple way of expressing the leading order solution for the correlations in the network. Let us consider the difference between the normalized instantaneous activities of the excitatory and inhibitory populations $m_\alpha(t) = \sum_i \sigma_i^\alpha(t)/N$ and the instantaneous activity of the external population, given by

$$\Delta_{\alpha X}(t) \equiv \frac{1}{A_\alpha m_X} (\sum_i \sigma_i^\alpha(t)/N) - \frac{1}{m_X} (\sum_i \sigma_i^X(t)/N) \qquad\qquad \alpha = E, I$$

We can measure the degree to which the activity in the recurrent network tracks the instantaneous activity in the external population by calculating the variance of $\Delta_{\alpha X}(t)$ at equilibrium,

$$\langle (\Delta_{\alpha X}(t) - \langle \Delta_{\alpha X}(t) \rangle)^2 \rangle = \frac{1}{N m_X^2} \left((a_\alpha + (N-1) r_{\alpha\alpha})/A_\alpha^2 + a_X - 2N r_{\alpha X}/A_\alpha \right)$$

Replacing expressions (38-39) into this formula one obtains that, to leading order, it vanishes. Similarly, it is simple to show in the same way that the variance of $\Delta_{EI}(t)$ also vanishes to leading order.

Thus, although the magnitude of the temporal fluctuations of the instantaneous firing rate of each population is $\sim O(\epsilon)$, the magnitude of the temporal fluctuations of the instantaneous *difference* in firing rates is $\sim O(\epsilon^{3/2})$. This implies that as the network gets larger, the instantaneous firing rate in the three populations track each other more faithfully, and that, asymptotically, tracking is *perfect*, i.e., as $N \to \infty$

$$\begin{aligned}
m_E(t) &= A_E \, m_X(t) \qquad (40) \\
m_I(t) &= A_I \, m_X(t) \qquad (41)
\end{aligned}$$

This result captures the essential difference between the sparse balanced network (*2,42*) and the densely-connected one. In the sparse balanced network, the recurrent feedback results in linear propagation of the average firing rate. In the dense network, not only the average firing rate, but also the instantaneous fluctuations in activity are faithfully propagated. In these conditions, referring to the average firing rate as 'signal' and to the fast temporal fluctuations as 'noise' becomes questionable, since both are propagated with the same accuracy.

Although we have assumed throughout that neurons from the external population were independent, this assumption can be relaxed. We assumed neurons in the X network were independent in order to avoid having to define the correlation structure of the external network *ad hoc*. Our results, however, are still valid if the external neurons are not independent, as long as the external network is itself asynchronous. Note that this does not qualitatively change the properties of the external input. Simply the existence of common input makes the average correlation between the external component of the synaptic input $\sim O(1)$. Thus, as long as the population-averaged correlation between the external neurons is $\sim O(1/N)$, this will only lead to quantitative changes in the correlation structure of the input from the external network. Hence, asynchronous activity self-consistently propagates within and across densely connected, strongly coupled networks (*46*). Asymptotic expressions for how rates and correlations propagate from one asynchronous network to another can be derived from a straightforward extension of the simple equations (40-41) to the case of two asynchronous networks, with network 2 receiving excitation from network 1. In the large N limit, it holds that

$$\begin{aligned} m_{E_2}(t) &= A_E^{1\to 2}\, m_{E_1}(t) \\ m_{I_2}(t) &= A_I^{1\to 2}\, m_{E_1}(t) \end{aligned}$$

Equations for the transformation of rates and correlations can be readily obtained by equating the temporal average, variance and covariance of the previous expressions

2.5 Balance of current correlations

The leading order solution for the average pair-wise correlations in the network leads to a cancellation between the different components of the average correlation between the currents to a pair of neurons. To see this, one just needs to note that

$$c_{ij}^{\alpha\beta} \equiv \langle \delta h_i^\alpha \delta h_j^\beta \rangle = \sum_{\gamma_k} A_{ik}^{\alpha\gamma} (J_{kj}^{\gamma\beta})^t$$

Thus, the average correlation between the synaptic currents to cells in populations α and β is equal to

$$c_{\alpha\beta} = \sum_\gamma J_{\alpha\gamma} a_\gamma J_{\gamma\beta}^t + \frac{1}{\epsilon^2} \sum_{\gamma\lambda} J_{\alpha\lambda} r_{\lambda\gamma} J_{\gamma\beta}^t \tag{42}$$

Terms proportional to a_γ in the previous sum are the contribution of shared input to the average current correlation. The other terms measure the contribution of correlations between pre-synaptic inputs to the average current correlation. Given that the leading order of the population-averaged correlations in firing

activity is $\sim O(\epsilon^2)$, the leading order of each term in the previous sum is of order unity. However, it is straightforward to check that if one substitutes the solution in equations (38-39) into equation (42), the positive and negative terms cancel out. Thus,

$$c_{\alpha\beta} \sim O(\epsilon) \tag{43}$$

Just as linear propagation of average firing rates in the sparse network is extended to linear propagation of instantaneous firing rates in the dense network, the cancellation of the mean excitatory and inhibitory synaptic inputs in the sparse network is extended to a cancellation of the positive components of the population-averaged current correlation (arising from shared input and from network amplification of correlations between excitatory cells and between interneurons), and a negative term coming from network amplification of the correlations that tracking induces between the excitatory and inhibitory cells.

The structure of the synaptic current correlations is very different in *sparsely* connected networks such as (*2,33*). In these networks each component of the current correlation in equation (42), including those arising from shared input, decrease with the network size in an asynchronous state. Thus, in a sparsely connected network the asynchronous state is a static feature of the network architecture, whereas in a densely connected network it is a purely dynamical phenomenon.

3 Supplementary Results

3.1 Impact of correlations on the instantaneous population activity

In this section we discuss the relationship between the (average) magnitude of spiking correlations across a neural population and the magnitude of the temporal fluctuations in its instantaneous activity. This relationship has been used to clarify the conditions under which spiking correlations have a significant impact on the accuracy with which the instantaneous activity of the population can be decoded (*32, 47, 48*). For completeness with the goal of our study, we illustrate this point graphically on this section.

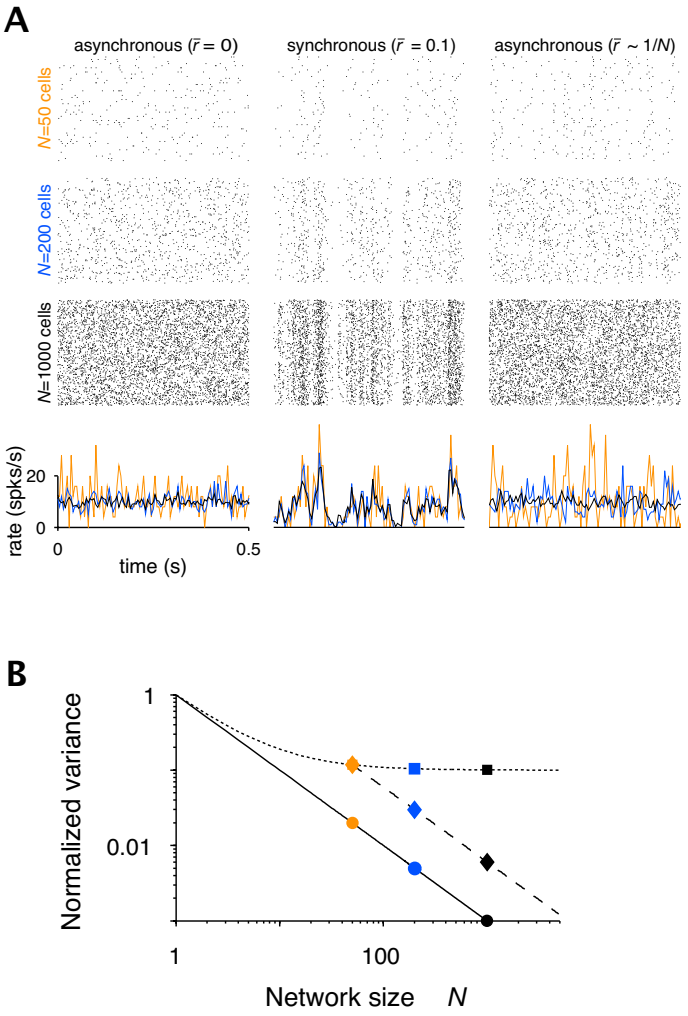

Fig. S2: Impact of the average correlation on the instantaneous population activity . **(A)** Spike rasters (top three rows) and traces of the instantaneous population activity $m(t)$ (fourth row) for networks of increasing size N (see colored labels by the rasters) and different correlations: independent cells, $\bar{r} = 0$ (left column), size-independent correlations, $\bar{r} = 0.1$ (center) and correlations which decay in a way inversely proportional to the network size, $\bar{r} = 5/N$ (right). Correlated spike trains were generated as in Fig. 1 (section 1.1.2). Population

activity $m(t)$ was obtained using a bin $dt = 5$ ms and normalized by dt to yield units of spikes per second. **(B)** Normalized temporal variance of the instantaneous activity $m(t)$ (equation 44) vs. network size N. In both the case with $\bar{r} = 0$ (solid) and $\bar{r} \sim 1/N$ (dashed), the variance decreases as $1/N$, whereas when $\bar{r} = 0.1$ (dotted) the variance saturates to $\sqrt{\bar{r}}$. Symbols represent the examples shown in (A) using the same color code.

Let us consider a network composed of N cells with firing rate $\bar{m}$ and pair-wise correlation $\bar{r}$. Spike rasters of the activity of examples of such a network are shown in Fig. S2A for different network sizes N (different rows) and different $\bar{r}$'s (different columns). The instantaneous population activity $m(t) = \sum_i n_i(t)/N$, where $n_i(t)$ is the firing rate of the i-th cell in a time window $(t, t + dt)$, is shown for each network in Fig. S2A (bottom). The variance across time V of the mean activity of the population $m(t)$, normalized by the variance v of the activity of each cell is given, for $N \gg 1$, by

$$\frac{V}{v} = \frac{1}{N} + \bar{r} \tag{44}$$

The magnitude of V/v quantifies the error that a downstream structure (using simple averaging) would make in the estimation of the average activity of the population $\bar{m}$, or, more precisely, the decrease in such error for a population of size N relative to the error for a population of size $N = 1$. Thus, V/v measures the extent to which it is advantageous to combine the activity of N neurons when pooling their activity.

If neurons are independent ($\bar{r} = 0$; Fig S2A, left column), V/v decays as $\sim 1/N$ (Fig. S2B, solid), the standard scaling of the (squared) error of the mean of N independent samples. Networks were the error of $\bar{m}$ decreases in this way were defined as *asynchronous* (*32*). If neurons in the network have a *fixed*, size-independent correlation $\bar{r} > 0$ (Fig S2A, center column), the error in the mean saturates to $\sqrt{\bar{r}}$ (Fig S2B, dotted) (*47, 48*). The smaller $\bar{r}$, the larger the size of the population at which the error starts to saturate, but for any size-independent $\bar{r}$, the error will always saturate nevertheless. We refer to networks with a size-independent $\bar{r}$ as *synchronous*. Notice that the distinction between synchronous and asynchronous networks defined this way is qualitative, as opposed to a situation where the degree of synchrony is assessed by the numerical value of $\bar{r}$. Although a network of independent neurons is asynchronous, not all asynchronous networks need to be composed of independent neurons. Equation (44) shows that a network of correlated neurons can be asynchronous as long the average correlation decreases with the network size as $\bar{r} \sim 1/N$ (Fig S2A, right column; B, dashed). Although correlations are present in such networks, they do not qualitatively affect the accuracy of the estimation of $\bar{m}$.

Given that the size N of a physiological network is fixed, what does it mean that the population-averaged correlation decreases as $\sim 1/N$? In other words, is it possible to tell whether a network *of a given size* is synchronous or asynchronous? Because the numerical value of $\bar{r}$ generated by an asynchronous network is small enough, it is always advantageous to consider more neurons in the network to estimate the instantaneous population activity. Thus, in an asynchronous network, the variance of the instantaneous activity of sub-popuations of size K decreases as $\sim 1/K$, whereas in a synchronous network, it would start to saturate at a value of $K < N$ (*32*).

3.2 The effect of shared inputs and correlated inputs cancels in recurrent networks

In this section we describe in more detail the way in which the effect of shared input is cancelled by the effect of correlations between inputs in the recurrent network studied in Fig. 2 of the main text (which we will refer to as RecN in this section). We start by showing explicitly that the net contribution of correlations in firing to the total current correlation c is negative, and that it cancels the positive contribution to c due to shared input. To do this, we first isolate each of the two effects.

To isolate effect of shared input, we considered a simulated two-layer feedforward network. Neurons in the first layer were independent and had firing rates equal to those of the RecN. By creating the synaptic connections from the first layer to the read-out population using exactly the same probabilistic rule as in the RecN (equation (11)), the correlations between currents to cells in the read-out population are equal to the correlations produced exclusively by shared input in the RecN. As expected, the distribution of these correlations is centered at $p = 0.2$, the average shared input fraction in the RecN (Fig. S3A, blue).

To isolate the effect of correlations in firing, we considered two read-out populations. Each of them received inputs exclusively from a different half of the RecN, and the synaptic connections to each population were again created by using the rule in equation (11), except that the probability of connection was doubled $p' = 2p$. By construction, neurons in different read-out populations share no inputs, but the synaptic current to each of them is statistically identical to the synaptic current to any cell in the RecN. Thus, correlations between the synaptic currents to cells of different read-out populations reflect exclusively the effect of correlations in firing in the RecN. Although correlations in firing contribute both positively and negatively to c (with E-E and I-I correlations contributing positively, and E-I correlations contributing negatively; Fig. 1D, F of the main text) the pink histogram in Fig. S3A shows that their net effect is negative, with mean slightly larger than - p. As described in the main text, the effects of shared input and of correlations in firing in the RecN cancel each other out (Fig. S3A, black), and the accuracy of this cancellation increases with the network size (Fig. 2C, black squares, Fig. 2E, and section 2.5 above). After the cancellation, shared input still explains some fraction of the variance in the distribution of current correlations (Fig. S3B, bottom; compare with the shared input only case, top, for a simulation of the same length). The fraction of variance explained by shared input is parameter dependent, but it does not go to zero with the network size.

An interesting functional consequence of the cancellation between the effects of shared input and correlated input is that it renders the firing correlation r_{ij} of a cell pair informative about the presence of direct connections between the two neurons. The effect of direct connections in our network is of the same order as their magnitude, $\sim 1\sqrt{N}$, which is small when compared separately to the net effect of shared input or to the effect of firing correlations between inputs, which are both independent of the network size. However, since these two large effects cancel, the resulting weak correlation c_{ij} is significantly affected by whether the neurons in the pair are connected or not. To show this, we plotted r_{ij} versus the fraction of shared input p_{ij} (*49*) for EI pairs in the RecN, using a different color for unconnected pairs (gray), and pairs with only a direct excitatory (green) or inhibitory (red) connection. We considered the firing correlation r_{ij} instead of the current correlation c_{ij} for this analysis because it reveals the effect of direct connections more explicitly. This is because direct connections have a stronger

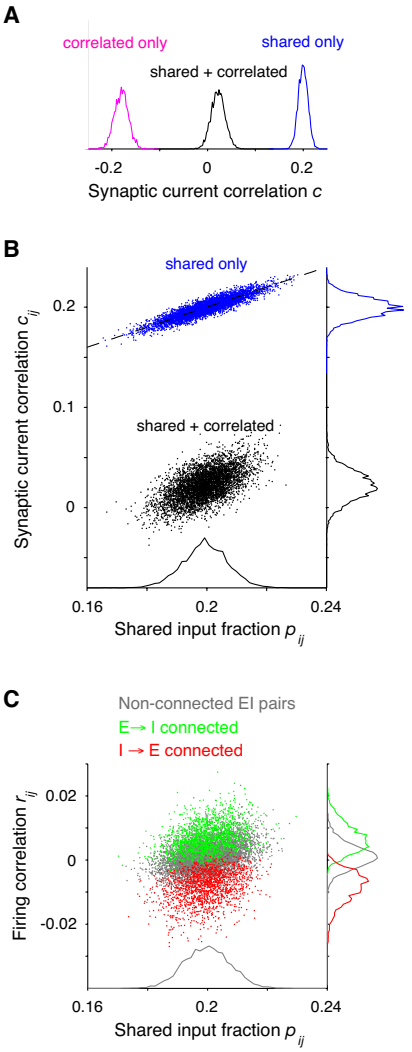

Fig. S3: Cancellation between correlations induced by shared inputs and correlated inputs. **(A)** Histograms of the correlation coefficient of the synaptic current c which reveal the contribution of only shared inputs (blue) or only firing correlations between inputs (pink) to the total current correlation (black) in the recurrent network presented in Fig. 2 (N = 4096) of the main text (see text for details). **(B)** Correlation c_{ij} of individual EE pairs vs. their shared input fraction p_{ij} for the recurrent network (black). Same but for the case with no correlations between inputs (see text) shown in blue. Dashed line is the diagonal $c_{ij} = p_{ij}$. **(C)** Firing correlation coefficient r_{ij} of EI pairs vs. p_{ij} for unconnected pairs (gray) and pairs with only a direct excitatory (green) or only a direct inhibitory (red) connection. We used 100 E cells in (A-B) and 50 E plus 50 I cells in (C). Simulations lasted $200,000$ and 10^6 τ's in (A) and (B-C) respectively.

effect on lagged than on instantaneous current correlations. Since the r_{ij} reflect the time integral of the whole current cross-correlogram, they are sensitive to the lagged correlations between synaptic currents. The correlations in firing r_{ij} clearly depend on the existence and type of direct connection between the cells (Fig. S3C, vertical colored histograms. Note that the area under this histograms has been normalized; there are many more unconnected (gray) than connected (red and green) pairs). Since whether a pair is or not connected is independent from its shared input fraction, p_{ij} explains a lower fraction of variance of r_{ij} than of c_{ij}, as the former is also strongly dependent on direct connections between the two cells. Exactly how informative r_{ij} is about the three sources of correlation in the network (fraction of shared input, magnitude and temporal structure of firing correlations between pre-synaptic inputs and direct connections between the neurons in the pair) is parameter-dependent, but it is a robust property of the network that all three effects have a significant impact on r_{ij} even asymptotically.

3.3 Robustness of the asynchronous state in the binary network

Since the cancellation between the different sources of positive and negative current correlations in the network is the result of a *dynamic* mechanism, it is expected that the existence of the asynchronous state should not depend in a sensitive way on the parameters which characterize the network architecture. Wi-

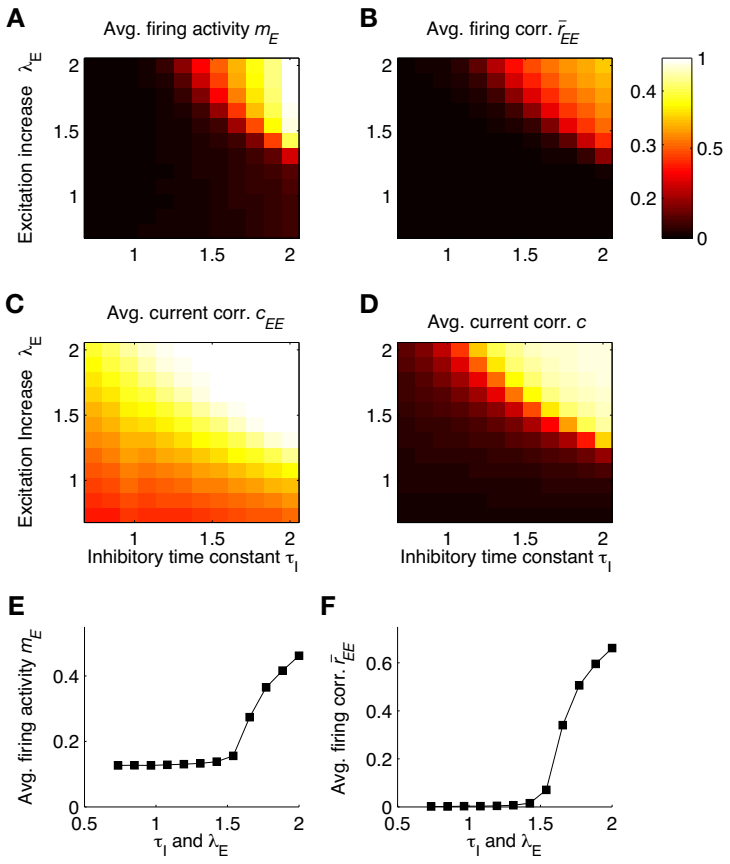

Fig. S4: Robustness of the Asynchronous state in the binary network. **(A)** Population-averaged excitatory activity m_E, **(B)** average firing correlation $\bar{r}_{EE}$, **(C-D)** average correlation between the excitatory currents c_{EE} (C) and between the total currents (D) onto E cells, plotted in color as the strength of the excitatory connections λ_E and the inhibitory time-constant τ_I are varied. The excitatory time constant was $\tau_E = 1$. At each point in the plot, the two recurrent excitatory synaptic couplings are equal to $\lambda_E j_{\alpha E}$, with $\alpha = E, I$, where $j_{\alpha E}$ are the values used in Fig. 2 of the main text (see section 1.1.1). The network in Fig. 2 corresponds to the point $\lambda_E = \tau_I = 1$ on these plots. Left colorbar scale applies to (A) and right colorbar scale applies to (B-D). **(E)** Average activity m_E along the $\tau_I = \lambda_E$ diagonal in (A). **(F)** Same as (E) but for $\bar{r}_{EE}$. Only properties of the activity of the E population are shown but the behavior of the I population is qualitatively identical. Statistics reflect the average over 10-20 networks ($N = 1024$) simulated for 200,000 τ_E.

thin a broad range, changes in the architecture lead to readjustments in the mean level of activity and the structure of fluctuations in such a way that the network remains balanced and asynchronous. In order for the inhibitory feedback to be effective, however, a minimum strength and speed of inhibition relative to excitation is needed. We explored the robustness of the asynchronous state numerically by examining the behavior of the network as the level of recurrent excitation and the inhibitory time-constant were increased. Recurrent excitation was increased by multiplying the two excitatory synaptic couplings $j_{\alpha E}$, $\alpha = E, I$ by the same factor λ_E. We also increased the time constant of inhibition τ_I relative to that of excitation which was fixed at $\tau_E = 1$.

The asynchronous state is stable for a wide range of values of λ_E and τ_I, but eventually becomes unstable when either inhibition becomes too weak or too slow compared to excitation (Fig. S4A-D). If one restricts the analysis to cases where $\lambda_E = \tau_I$, the asynchronous state becomes unstable beyond a critical value $\lambda_E = \tau_I \simeq 1.5$ (Fig. S4E-F). Beyond this point the inhibitory feedback is not efficient enough and the network activity displays large amplitude oscillations.

3.4 Effect of time-varying external inputs on correlations in the binary network

Our theoretical analysis was restricted to stationary conditions, i.e., constant firing rates of neurons in the X population. This situation however, is very restrictive. Although we have shown that the activated state under urethane anesthesia is well described by essentially stationary spiking (Fig. 4 main text), firing rates are generally expected to change in time, either due to internal dynamics under anesthesia or due to sensory stimuli, motor behavior or cognitive processing during wakefulness. We investigated numerically whether an asynchronous network state similar to that described in the main text, is also possible under time-varying inputs. Since the tracking of random fluctuations by the network is very fast, we expect that if the mean external input does not change too quickly, tracking of fluctuations will still take place *on top* of the time-varing signal, resulting in an active decorrelation of synaptic currents even in these conditions.

We tested this hypothesis by modulating the firing rate of the external inputs to the recurrent network. We used a periodic (filtered white noise, period 1 s = 100 neuronal time-constants) stimulus $\overline{m}^X(t)$ (equation (18)) which repeated 1000 times (Fig. S5A shows 10 repetitions). This time-varying input induced global temporal modulations in the activity of the whole network (Fig. S5A, C) of a significantly larger magnitude that the random fluctuations present when the input is stationary (Fig. S5B). Because the modulation was periodic, we could compute the instantaneous average activity of each neuron across repetitions (Fig. S5C). As expected, disregarding the global activity modulation and simply calculating correlations with respect to the mean activity of each cell across the whole simulation leads to a distribution of firing correlations r biased towards positive values (Fig. S5D, red). However, if covariations in activity are measured with respect to the time-varying average activity of each neuron (Fig. S5C), the positive bias in the correlation histogram is removed (Fig. S5D, orange), resulting in a distribution of r very similar to that obtained under stationary conditions (Fig. S5D, blue). This is consistent with our finding that the positive bias in the distribution of correlations during the inactivated state (Fig. 4D main text) is removed when one restricts the analysis to activity during Up-states (Fig. 4D-F).

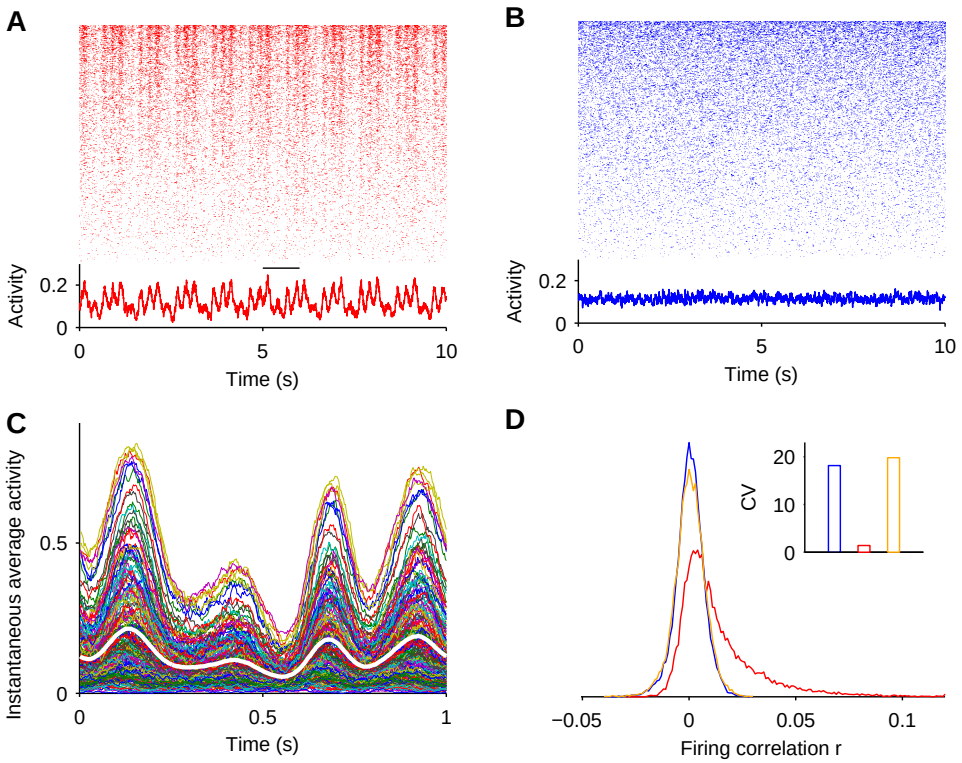

Fig. S5: Asynchronous activity under non-stationary conditions. **(A)** Raster of 500 neurons (top, sorted by rate) and instantaneous mean population activity (bottom, N = 4096). The firing rate of the external population was periodically modulated in time, causing global fluctuations in the instantaneous activity of the recurrent network (period = 1 s, horizontal bar). **(B)** Same as (A) for a stationary external input, as used in Fig. 2 of the main text. **(C)** Average instantaneous activity of a random subset of 200 neurons in (A) across 1000 repetitions of the time-varying signal. Thick white line is the mean of the average instantaneous activity across the 200 cells. **(D)** Histogram of firing correlations r for the different stimulation conditions. Correlations displayed in the blue and red histograms represent covariations in the activity of pairs of neurons with respect to their average activity across the whole simulation (1000 s) for networks driven by stationary and time-varying inputs respectively. Conditioning on the instantaneous average activity of each cell (color lines in (C)) removes the positive bias of the distribution of correlations, revealing asynchronous activity under a non-stationary situation (orange). Inset: coefficient of variation (CV = $\sigma_r/\bar{r}$) of the three histograms. The histogram of correlations is wide both under stationary conditions and time-varing conditions as long as correlations are conditional on the time-varying signal.

Thus, large global activity modulations are compatible with the mechanism for active decorrelation of synaptic inputs described in the main text. This is not a trivial result. In fact, in this network, if the external inputs change sufficiently fast, they interfere with the tracking or random fluctuations, resulting in a positive bias in the distribution of correlations even after conditioning on the average instantaneous activity of the neurons (data not shown; but see Fig. S8).

3.5 Robustness of asynchronous activity in the spiking network

In section 3.3 we showed that asynchronous activity occurred robustly for a large range of parameters in the binary network. We now show that the key characteristics of asynchronous activity, namely weak total current correlations when compared to the temporal correlations of the individual current components and a wide distribution of spiking correlations, are also robust features of spiking networks of integrate-and-fire neurons.

We start by providing a detailed characterization of the activity of the spiking network shown in Fig. 3 of the main text. Neurons in the network fire tonically and irregularly, with the membrane potential hovering below threshold and with large fluctuations occasionally driving spikes (Fig. S6A). The distribution of spike count correlations r is wide ($\sigma_r \gg \bar{r}$) for all three cell pair types, but especially for II pairs (Fig. S6B). Both the positive and the negative tails of the r distribution are not present in the jittered data and are therefore generated by the network dynamics, rather than reflecting estimation errors due to the finite length of the simulations. We investigated the dependency of the mean $\bar{r}$ and width σ_r of the correlation histogram on the count window T (Fig. S6C-D). As T goes to zero, all spiking correlations trivially vanish (*50*). Very short-time correlations are on average all positive and increase with T up to a few ms, at which point they start decreasing, reaching a low asymptotic value at $T \simeq 20$ ms which does not change as T is increased further (Fig. S6C). Additionally, the width of the correlation histogram for all three cell-pair types relative to the jittered surrogates, has a maximum as a function of T (Fig. S6D). Both of these results can be understood as follows. The spike count covariance with count window T is related to the area under the cross-correlogram (CCG) of the corresponding spike trains in the interval $(-T, T)$ (see e.g. (*51*)). For two finite, independent spike trains, the spike count covariance would therefore reflect the integration of statistical fluctuations, and so have zero mean and a variance that grows with T. For two correlated spike trains whose CCG has width τ_{CCG}, the spike count covariance when $T < \tau_{CCG}$ is related to the shape of the CCG. As T becomes much larger than τ_{CCG}, the value of the covariance does not change on average (Fig. S6C), but its estimation becomes less accuarate as a larger fraction of the covariance reflects integration of 'noise' (*28*). Because in this network $\tau_{CCG} \simeq 20$ ms (Fig. S6E), as $T \gg 20$ ms, $\bar{r}$ reaches a plateau (Fig. 6C) and σ_r approaches the width of the histogram of jittered surrogates (Fig. S6D).

We next characterized in more detail the cancellation between the synaptic currrent correlations shown in Fig. 3C-D of the main text. Fig. S6F shows the CCGs between the different current components. The instantaneous correlation of the total current (i.e. the peak of the CCG) is smaller than that of the components. Although this effect is qualitativelly similar to the cancellation of the correlations of the components of the membrane potential (Fig. 3C), the total current is comparatively more correlated than the membrane potential at rest (compare peaks of the black CCGs in Fig. 3C and Fig. S6F). In order to understand the relationship between synaptic current and membrane potential correlations, we computed the correlation between the currents filtered using a simple causal exponential filter of time constant τ_f (*52*). While the correlation between the filtered current components remains large for all values of τ_f, the filtered total currents become less and less correlated as τ_f increases (Fig. S6G) due to the fact that the area under the negative side lobes in the CCG of the total current is almost the same as

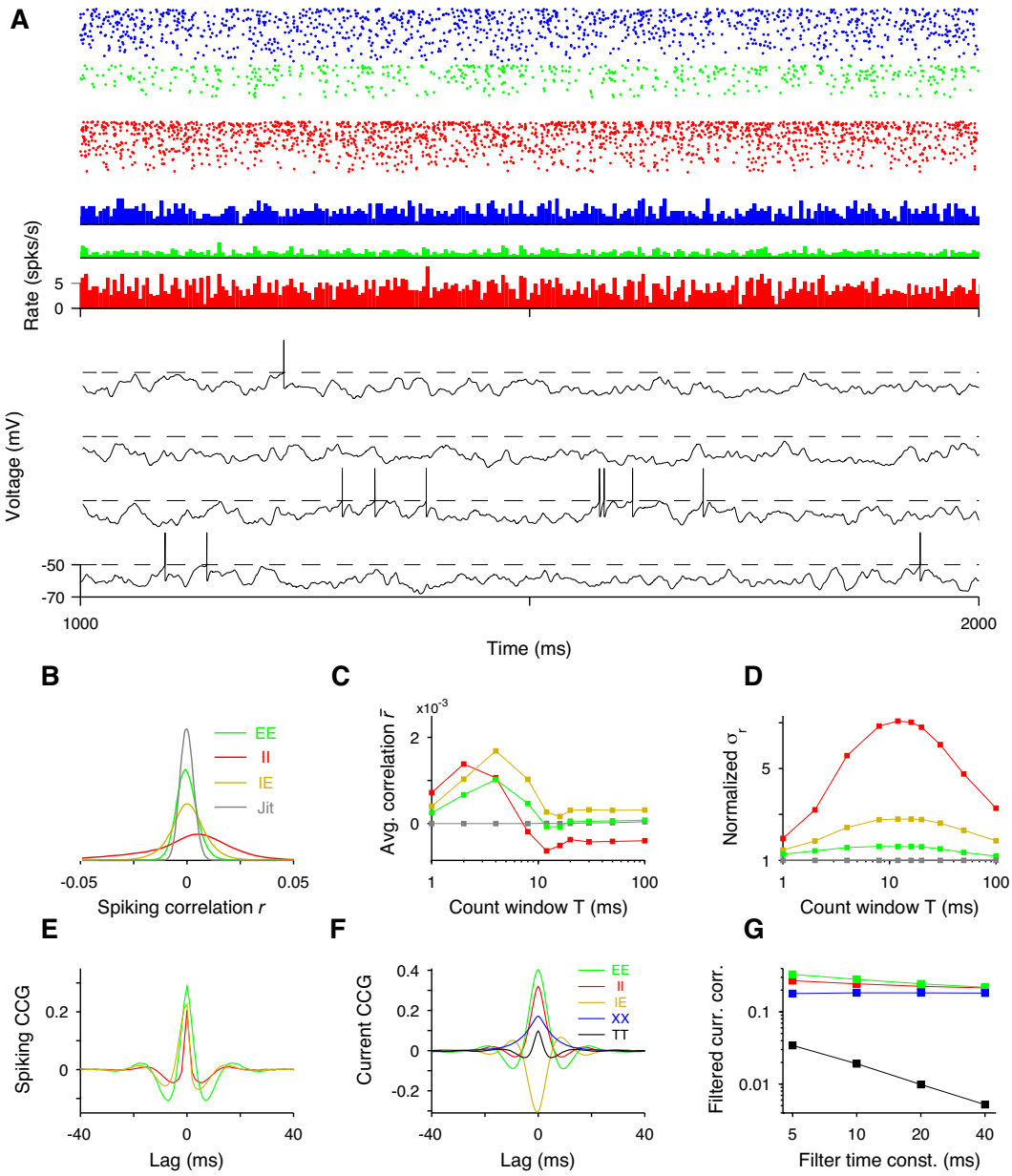

Fig. S6: Asynchronous activity in a recurrent network of spiking neurons. **(A)** Spike rastergrams of 500 neurons (sorted by rate) from the external (blue), excitatory (green) and inhibitory (red) populations (top), instantaneous activity of each population (middle, bin size 4 ms) and example voltage traces of two E (first and second) and two I (third and fourth) neurons (bottom). **(B)** Histograms of the spike count correlation coefficients r of the different types of cell pairs and the jittered spike trains (count window $T = 20$ ms). Jittered surrogates were constructed by adding a uniform random variable in [-0.5, 0.5] s to each spike. **(C)** Average spiking correlation $\bar{r}$ vs. count window T. **(D)** Standard deviation σ_r of the data normalized by that of the jittered surrogates vs. T. **(E)** Average spike cross-correlograms of each pair type (from a random subset of 1000 E and 1000 I cells) computed by subtracting one from equation (9). **(F)** Average current CCG for different current component pairs. **(G)** Average

correlation coefficient of the filtered currents vs. the filter time constant (see text). All data comes from a single network simulated for 5000 s. All parameters as in Fig. 3 of the main text (values given in section 1.1.2).

the area under the central peak, so that the total area is almost zero (*53*). Thus, similarly to the binary network (Fig. 2F steps *ii* and *iii*), the full cancelation of correlations in the spiking network seems to occur in two steps: first, when the different components are summed together and second, when the total current is integrated by the cell's membrane potential.

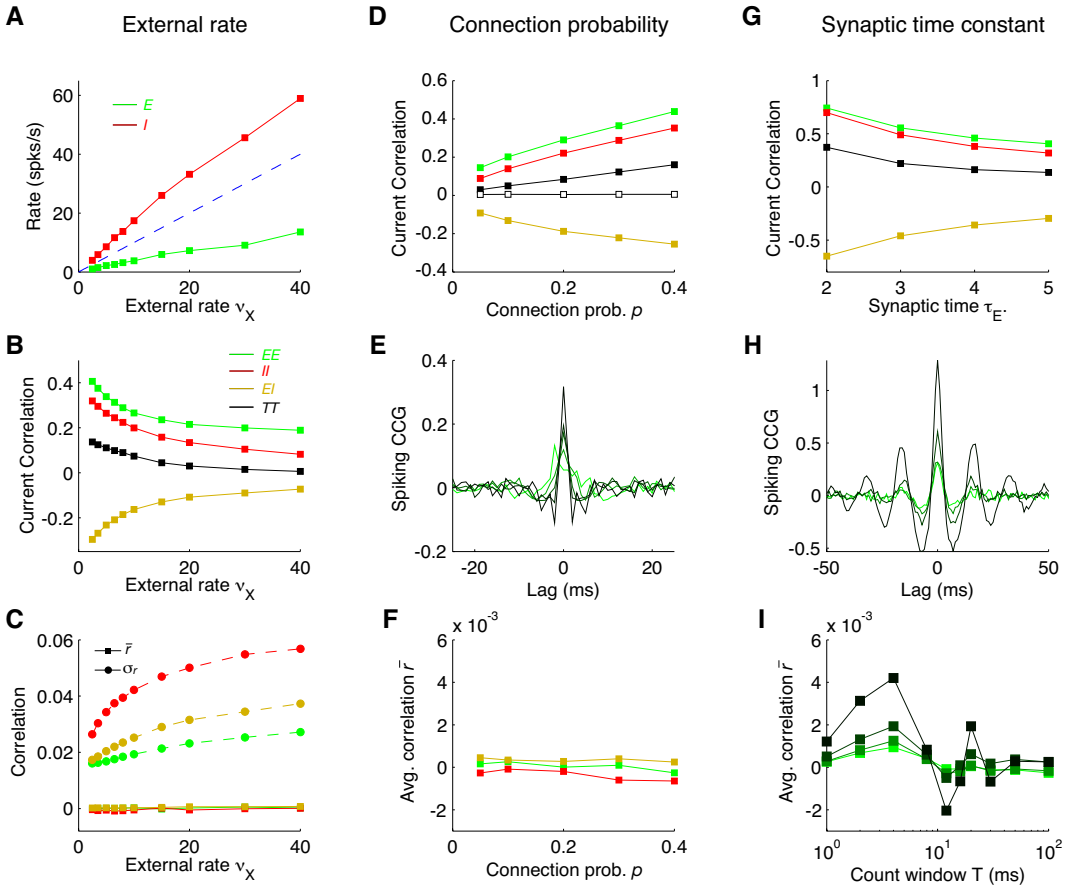

Fig. S7: Robustness of asynchronous activity in spiking networks. Left column: Effect of changing the external rate ν_X on **(A)** the mean rate of the network, **(B)** the averaged correlation of the current components, and **(C)** the mean $\bar{r}$ and std. dev. σ_r of the spike count correlations. **Middle column:** Effect of changing the probability of connection p in the network on **(D)** the correlation of the current components (white squares represent the correlation of the filtered currents, τ_f = 20 ms), **(E)** the population-averaged spiking CCGs of EE pairs (computed as in Fig. S6E), with lighter color corresponding to lower p, and **(F)** $\bar{r}$. **Right column:** Effect of decreasing the excitatory synaptic decay time constant τ_E (both recurrent and external). **(G, H)** Same as (D, E). **(I)** Averaged correlation $\bar{r}$ between EE pairs as a function of the spike count window. In (H, I) lighter colors correspond to

longer τ_E's. All data are averages over 5-10 networks simulated for 200 s. All fixed parameters as in Fig. 3 except for $\nu_X = 8$ spks/s (middle column). Count window T = 20 ms in (C, F).

The effect of changing several network parameters on the behavior of the network just described is shown in Fig. S7. Increasing the external drive to the network (Fig. S7, left column) increases the firing rate of the recurrent neurons in an approximately linear fashion (Fig. S7A), as is typical in balanced networks (*2*, *54*). Overall, population-averaged synaptic currents become less correlated as the firing rates increase (Fig. S7B). Higher firing rates lead to wider distribution of spiking correlations with average correlations qualitatively unaffected (Fig. S7C; see also Fig. S8D). Next we examined the effect of changing the probability of connection p (Fig. S7, middle column). The correlation between the current components and between the total currents (albeit more slowly) grows with p (Fig. S7D). However, the negative side-lobes of the total current CCG grow in parallel (Fig. S7E), in such a way that the instantaneous correlation of the filtered total synaptic current (filter time-constant τ_f = 20 ms) (Fig. S7D, white squares) and the population-averaged spike count correlation $\bar{r}$ (Fig. S7F) do not change with p. This is further evidence that $\bar{r}$ is set dynamically and is not determined by the level of shared input in the network. Finally, we shortened the synaptic decay time constant τ_E of the excitatory synapses (Fig. S7, right column). As expected, when excitation becomes progressively faster than inhibition (in Fig. S7G-I, τ_I = 5 ms) the negative feedback is not fast enough and the network becomes more synchronized. Instantaneous current correlations, including the correlations between the total synaptic currents, increase (Fig S7G). Average spike train CCGs also grow in magnitude and acquire a more oscillatory character (Fig. S7H). Nevertheless, this increase in oscillatory synchrony is gradual (no sharp transitions in the qualitative behavior of the network were observed) and has a relatively mild impact on the population-averaged spike count correlations (Fig. S7I).

3.6 Effect of time-varying external inputs on correlations in the spiking network

In this section we study the behavior of correlations under non-stationary conditions in the network of conductance-based integrate and fire neurons. We investigated this issue by having the instantaneous firing rate of the external neurons ν_X oscillate sinusoidally ($\nu_X(t) = 15 + 10\sin(2\pi f t)$ spks/s), and by measuring how correlations in the network depended on the frequency of the oscillation f.

As expected in a balanced network (*2*), the mean rate of the E and I populations follows accurately the temporal modulation of the external input (Fig. S8A) (*55*). Spike train CCGs were corrected for the modulation of the mean rate using a shift predictor: we obtained the CCG for each pair of spike trains following equation (9) and then subtracted a CCG obtained using the same formula but shifting the two trains by a random integer number of oscillation periods (*28*). The peak of the population-averaged CCG between EE pairs remained constant for $f < 10$ Hz and then it increased by a factor of ~ 3 between 10 and 100 Hz (Fig. S8B). Spike count correlations increased correspondingly, especially for very short count windows, although overall they remained very small on average (Fig. S8C). Thus, although as expected tracking becomes less effective when the external inputs change rapidly, this does not have a strong impact on $\bar{r}$. This does not mean, however, that the correlation structure of the network is unaffec-

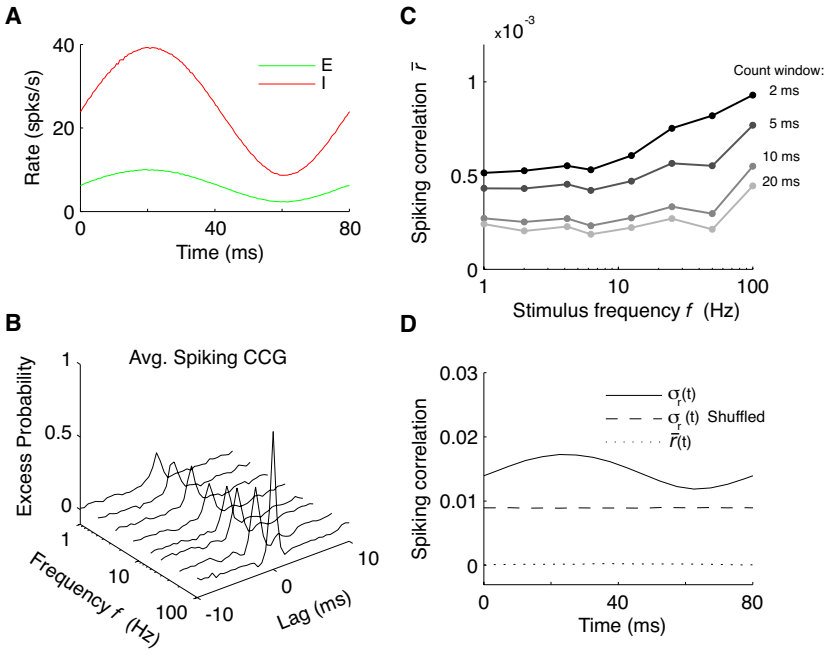

Fig. S8: Asynchronous activity in the spiking network in the presence of sinusoidal time-varying inputs. The external rate was varied sinusoidally over a range of frequencies f from 1 to 100 Hz. **(A)** Instantaneous average firing rates of the E and I populations as a function of time for a stimulus with f = 12.5 Hz (*55*). **(B)** Population-averaged shift corrected CCG of EE pairs (see text). The CCG peak increases with f. **(C)** Population-averaged spike count correlation $\bar{r}$ for EE pairs as a function of f for different spike count windows. **(D)** Instantaneous mean $\bar{r}(t)$ and std. dev. $\sigma_r(t)$ of EE pairs as a function of time (f = 12.5 Hz, count window T = 20 ms). The width $\sigma_r(t)$ follows the mean firing rate (see also Fig. S7C). Dashed line represents the correlation std. dev. for the shuffled data (see text). Data shown are averages over sets of 200 E and 200 I neurons chosen from each of four networks simulated for 1000 s. All parameters as in Fig. 3.

ted by the input. To show this, we computed the population-averaged instantaneous spike count correlation $\bar{r}(t)$ and the instantaneous std. dev. $\sigma_r(t)$ as a function of time during an oscillation period using sliding count windows of T = 20 ms (Fig. S8D, sliding step 5 ms). We also computed $\sigma_r(t)$ for the shuffled data set obtained by shifting the spike trains as described above. The std. dev. $\sigma_r(t)$ from the data was larger than that of the shuffled data, and was modulated in time, to a much larger extent than $\bar{r}(t)$ (at the scale of the plot, $\bar{r}(t)$ appears constant). Thus, correlations increase transiently in magnitude during epochs of high rate, but positive and negative correlations increase similarly with rate, resulting in a very weak modulation of $\bar{r}(t)$. This qualitative behavior was observed for the whole range of frequencies studied. The small values of $\bar{r}(t)$ obtained are not a consequence of the method employed to measure spiking correlations. Feed-forward networks of integrate-and-fire cells firing at similar rates can exhibit correlation coefficients r in the range 0.1-0.2 (see, e.g., Fig. 1E) which can be largely and quickly modulated by time-varying inputs (*56*). We therefore conclude that asynchronous activity is a robust feature of the spiking network even in the presence of time-varying inputs.

3.7 Time-scale dependence of correlations in the rat cortex *in vivo*

To verify that our conclusions regarding the distributions of correlations from the *in vivo* population recordings were not dependent on any specific counting window T, we repeated the analyses using different values of T. Correlation coefficients were calculated as described in Section 1.3.4, keeping the jitter interval J fixed to four times the counting window, i.e., $J = 4T$.

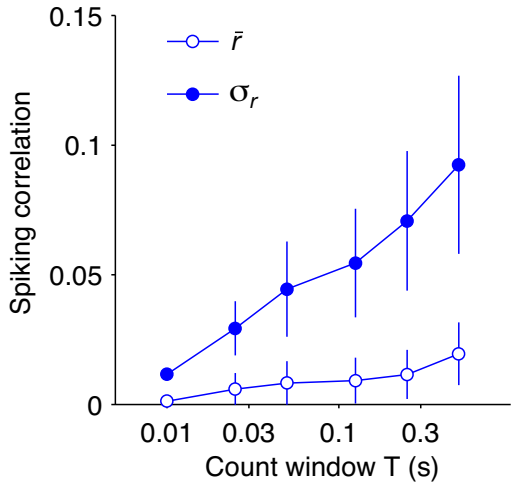

Fig. S9: Distribution of correlations at different time-scales. Empty and filled dots correspond to the average (plus minus standard deviation) across recording sessions of the mean correlation $\bar{r}$ and correlation histogram width σ_r respectively. The histogram is wide across a large range of counting windows. Notice the logarithmic scale in the x-axis.

Fig. S9 shows the average across experiments of the mean $\bar{r}$ (empty circles) and std. dev. σ_r (filled circles) of distributions of correlations with time-scale T during the ACT state, for T ranging from 10 ms to 500 ms. Considering correlations at different time-scales T, does not lead to qualitative differences with the results presented in Fig. 4 of the main text (in which $T = 50$ ms): first, the mean correlation $\bar{r}$ was very small (less than 0.02) for all counting windows up to T = 500 ms, although it shows a slight increasing tendency. Second, the coefficient of variation of the distribution is also large for all windows on this range, showing that the distribution of correlations being wide is not crucially dependent on the time-scale at which correlations are measured.

As expected, the width of the histogram goes to zero with decreasing T, since spike count correlations become linear in the counting window as $T \to 0$ (*50*). At the other extreme, correlations tend to become more positive on time-scales of the order of seconds. However, such slow covariations in activity are expected to reflect processes other than synaptic transmission and integration (which are in general one to two orders of magnitude faster).

3.8 Examples of CCGs of individual cell pairs in the rat cortex *in vivo*

To investigate the temporal structure of pairwise correlations on fine time-scales we computed individual cross-correlograms (CCGs, equation 9) from the experiment illustrated in Fig. 4A-B of the main text, during the ACT period (Fig. S10).

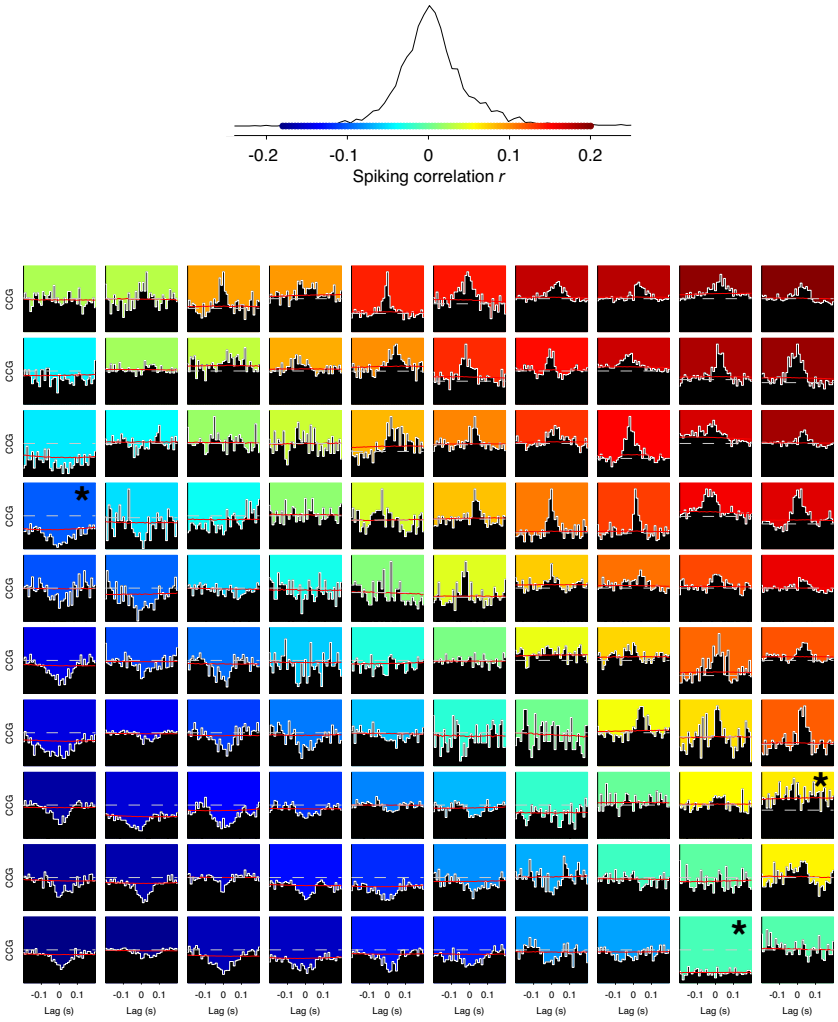

Fig. S10: Examples of individual CCGs. One hundred raw CCGs (equation 9, bin size dt= 10 ms) from the experiment shown in Fig. 4A-B of the main text. CCGs where chosen to span the whole range of correlations observed for this experiment. Top, distribution of correlations r for this experiment (identical to the one in Fig. 4B; count window $T = 50$ ms). The color scale for r is shown horizontally. Bottom, array of individual CCGs arranged according to the r value of each pair, which is also shown as the background color (see color bar on top). The gray dashed lines mark the value 1 which signals no correlation when the trains are stationary. The red lines shows the average CCG across 1000 jittered surrogates (jitter interval J= 200 ms). Only pairs with geometric mean

firing rate $\sqrt{\nu_i \nu_j} > 1$ spikes/s were considered. The y-axis of each plot goes from zero to the maximum between two and 1.1 times the CCG peak value. Asterisks show some examples with clear differences between the average of the jittered CCGs and one, i.e., pairs significantly correlated on slow time-scales.

Fig. S10 shows cross-correlograms for 100 pairs, with correlation coefficients equally spaced in the interval $r = (-0.18, 0.2)$, which almost spanned the whole range of values of r obtained in this experiment; specifically, we divided this interval in one hundred equi-spaced correlation values, and selected the pair with the closest r to each of those values. In order to avoid extremely sparse CCGs, we only chose pairs ij in which the geometric mean of the firing rates, $\sqrt{\nu_i \nu_j}$, was larger than 1 spike/s. We compared each raw CCG (white) with *(i)* a baseline value of one, expected if the two spike trains were stationary and independent (dashed gray lines) and *(ii)* with the baseline value expected if the two trains were only independent on time-scales $\ll 200$ ms (red lines, obtained as the average CCG across jittered surrogates for each pair of spike trains; see sections 1.3.4 and 1.3.6 for details). Because the method we used to compute r corrects for correlations produced by slow co-moduations of the rates, the figure shows that the sorting of pairs by r matches the comparison of each CCG with the baseline obtained from the jittered surrogate trains (asterisks show a few examples where the two baselines are clearly different, i.e., pairs correlated on slow time-scales).

As expected, pairs with positive r showed clear peaks in their CCGs and pairs with negative r showed clear troughs. Pairs with $r \simeq 0$ showed mostly flat CCGs although a few showed a combination of small peaks and troughs. Note that the CCGs of the pairs with the most negative r values have a symmetric trough around zero. Symmetric CCGs have been usually interpreted as being the result of anatomically shared input (*57–59*). However, both excitatory and inhibitory shared input can only induce *positive* correlations (Fig. 1A of the main text), i.e., CCG peaks. Thus, all of the symmetric troughs and many of the symmetric peaks are likely to be caused by specific combinations of positively and negatively correlated inputs, rather than anatomically shared inputs.

3.9 Distance dependence of correlations in the rat cortex *in vivo*

In order to investigate whether the distance between two cells in a pair has some influence over the measured value of their spiking correlation, we recomputed correlation histograms with pairs recorded a given number of shanks away from each other (see section 1.3.7) during periods of cortical activation. Since our silicon electrodes consist of 8 linearly arranged shanks separated by 200 μm each, the whole electrode array spans a considerable distance across the cortex (1.4 mm; all penetrations were normal to the cortex, i.e. shanks were perpendicular to the cortical layers). As shown in Fig. S11, only σ_r, but not $\bar{r}$, decreased with the distance (σ_r slope = - 0.017/mm, p < 0.001; $\bar{r}$ slope = - 0.002/mm, p = 0.35, p-values with respect to a null hypothesis of no distance dependence, see Section 1.3.7). Thus, distant pairs tended to be more weakly correlated (for both correlation signs), but there were still similar numbers of positively and negatively correlated pairs at all distances. The distribution of correlations is wider (relative to its mean) for neurons recorded in the same shank.

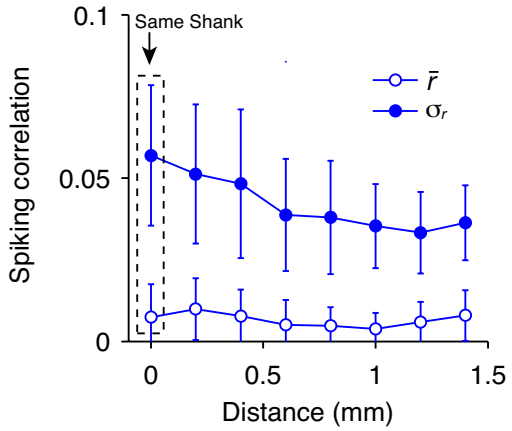

Fig. S11: Distance dependence of correlations. Mean correlation $\bar{r}$ (empty circles) and correlation histogram width σ_r (filled circles), as a function of the distance between the shanks where each of the neurons in the pair were recorded (the two curves show the average and std. dev. across recording sessions). Zero distance means both neurons were recorded in the same shank. The mean correlation $\bar{r}$ does not depend on the distance, but the correlation width σ_r does (see text).

References and Notes

1. D. J. Amit, *Modeling Brain Function* (Cambridge University Press, Cambridge, UK, 1989).
2. C. van Vreeswijk, H. Sompolinsky, *Science* **274**, 1724 (1996).
3. L. M. Ricciardi, *Diffusion processes and Related topics in biology* (Springer-Verlag, Berlin, 1977).
4. H. Tuckwell, *Introduction to Theoretical Neurobiology II* (Cambridge University Press, Cambridge, UK., 1988).
5. A. Kuhn, A. Aertsen, S. Rotter, *Neural Comp.* **15**, 67 (2003).
6. J. de la Rocha, N. Parga, *J. Neurosci.* **25**, 8416 (2005).
7. A. Compte, N. Brunel, P. Goldman-Rakic, X. Wang, *cc* **10**, 910 (2000).
8. N. Brunel, X.-J. Wang, *J Neurophysiol* **90**, 415 (2003).
9. A. Lerchner, M. Ahmadi, J. Hertz, *Neurocomputing* **58-60**, 935 (2004). Computational Neuroscience: Trends in Research 2004.
10. T. Vogels, L. Abbott, *J. Neurosci.* **25**, 10786 (2005).
11. S. El Boustani, M. Pospischil, M. Rudolph-Lilith, A. Destexhe, *Journal of Physiology-Paris* **101**, 99 (2007). Neuro-Computation: From Sensorimotor Integration to Computational Frameworks.
12. A. Kumar, S. Schrader, A. Aertsen, *Neural Computation* **20**, 1 (2008).
13. M. Matsumura, D.-f. Chen, T. Sawaguchi, K. Kubota, E. E. Fetz, *J. Neurosci.* **16**, 7757 (1996).
14. M. Ren, Y. Yoshimura, N. Takada, S. Horibe, Y. Komatsu, *Science* **316**, 758 (2007).
15. A. Hasenstaub, *et al.*, *Neuron* **47**, 423 (2005).
16. M. Okun, I. Lampl, *Nat Neurosci* **11**, 535 (2008).
17. P. Bartho, *et al.*, *J Neurophysiol* **92**, 600 (2004).
18. A. Luczak, P. Bartho, S. L. Marguet, G. Buzsaki, K. D. Harris, *Proceedings of the National Academy of Sciences* **104**, 347 (2007).
19. T. Klausberger, *et al.*, *Nature* **421**, 844 (2003).
20. K. D. Harris, D. A. Henze, J. Csicsvari, H. Hirase, G. Buzsaki, *J Neurophysiol* **84**, 401 (2000).
21. L. Dtri, D. D. Rasmusson, K. Semba, *Brain Research* **759**, 112 (1997).
22. M. Murakami, H. Kashiwadani, Y. Kirino, K. Mori, *Neuron* **46**, 285 (2005).
23. E. A. Clement, *et al.*, *PLoS ONE* **3**, e2004 (2008).

24. C. Y. Li, M. M. Poo, Y. Dan, *Science* **324**, 643 (2009).

25. M. Steriade, A. Nunez, F. Amzica, *J. Neurosci.* **13**, 3252 (1993).

26. M. Steriade, *Electroencephalography* (Williams and Willkins, 1999), fourth edn.

27. C. Curto, S. Sakata, V. Itskov, K. D. Harris, *J. Neurosci.* **29**, 10600 (2009).

28. W. Bair, E. Zohary, W. T. Newsome, *J. Neurosci.* **21**, 1676 (2001).

29. S. Fujisawa, A. Amarasingham, M. T. Harrison, G. Buzsaki, *Nat. Neurosci.* **11**, 823 (2008).

30. M. T. Harrison, S. Geman, *Neural Computation* **21**, 1244 (2009).

31. L. F. Abbott, C. van Vreeswijk, *Phys. Rev. E* **48**, 1483 (1993).

32. I. Ginzburg, H. Sompolinsky, *Phys. Rev. E* **50**, 3171 (1994).

33. D. J. Amit, N. Brunel, *Cerebral Cortex* **7**, 237 (1997).

34. N. Brunel, V. Hakim, *Neural Computation* **11**, 1621 (1999).

35. X.-J. Wang, *J. Neurosci.* **19**, 9587 (1999).

36. C. Meyer, C. v. Vreeswijk, *Neural Computation* **14**, 369 (2002).

37. D. Hansel, G. Mato, *Neural Computation* **15**, 1 (2003).

38. S. El Boustani, A. Destexhe, *Neural Computation* **21**, 46 (2009).

39. R. J. Glauber, *Journal of Mathematical Physics* **4**, 294 (1963).

40. J. A. Hertz, A. Krogh, R. G. Palmer, *Introduction to the theory of neural computation* (Addison-Wesley, Wokingham, U.K., 1991).

41. S. Ma, *Statistical Mechanics* (World Scientific, Singapore, 1985).

42. C. van Vreeswijk, H. Sompolinsky, *Neural Computation* **10**, 1321 (1998).

43. When averaging over $P(J)$, we will always make the assumption that the dynamical properties of neurons are independent of the particular realization of their output connectivity. We expect this to be a good approximation for large N in the asynchronous state.

44. Here, and in the following sections, the indices on the current variables $c_{\alpha\beta}$ refer to the population of the *post-synaptic* neurons. This notation is different from the one used in the main text, where c_{EE}, c_{II} and c_{EI} referred to the different components of total current correlation. For simplicity, we did not explicitly label the population of the post-synaptic neurons in the main text.

45. By this we mean that keeping track of terms $\sim O((A_{ij}^{\alpha\beta})^2)$ and $\sim O(B_{ij}^{\alpha\beta})$ does not change the leading order value of the population-averaged correlations that one obtains neglecting them.

46. Note, however, that if the activity in the external network is synchronous, i.e., $r_{XX} \sim O(1)$, tracking will not be able to produce asynchronous activity in the recurrent network. In this case, the covariance of the external current would be $\sim O(N)$, whereas the covariance of the E and I currents is $\sim O(1)$. Thus the negative term c_{EI} of the current covariance will never be large enough to cancel the term c_{XX} if the recurrent network is asynchronous and the external one is synchronous.

47. K. H. Britten, M. N. Shadlen, W. T. Newsome, J. A. Movshon, *J. Neurosci.* **12**, 4745 (1992).

48. E. Zohary, M. N. Shadlen, W. T. Newsome, *Nature* **370**, 140 (1994).

49. The fraction of shared inputs p_{ij} for a given pair is defined as the number of inputs projecting onto the two cells divided by the geometric mean of the number of inputs projecting to each. It has mean p and a std. dev. which decreases with network size as $\sim 1/\sqrt{N}$.

50. S. Panzeri, S. R. Schultz, A. Treves, E. T. Rolls, *Proceedings of the Royal Society of London. Series B: Biological Sciences* **266**, 1001 (1999).

51. T. Tetzlaff, *et al.*, *Neural Computation* **20**, 2133 (2008).

52. If $I(t)$ is the current component, the filtered current $I_f(t)$ is the solution of $dI_f(t)/dt = (I(t) - I_f(t))/\tau_f$.

53. The instantaneous correlation between two filtered variables equals the area under the cross-correlation function of the original variables multiplied by the (deterministic) cross-correlation function of the filter kernel (*51*).

54. N. Brunel, *J. Comput. Neurosci.* **8**, 183 (2000).

55. We did not observe a decrease in the amplitude of the oscillation in the network as the external frequency was increased, but the shape of the oscillation started to deviate from a perfect sinusoidal for the highest frequencies of 50 and 100 Hz.

56. E. Shea-Brown, K. Josic, J. de la Rocha, B. Doiron, *Physical Review Letters* **100**, 108102 (2008).

57. J.-M. Alonso, L. M. Martinez, *Nat Neurosci* **1**, 395 (1998).

58. M. D. Binder, R. K. Powers, *J Neurophysiol* **86**, 2266 (2001).

59. M. Eichler, R. Dahlhaus, J. Sandkühler, *Biological Cybernetics* **89**, 289 (2003).